1971

An experimental investigation of heat transfer to cones in rarified hypersonic flow.

Berry, Carl T.

Princeton University

AN EXPERIMENTAL INVESTIGATION OF HEAT TRANSFER TO CONES IN RAREFIED HYPERSONIC FLOW

Carl T. Berry

August 1971

AN EXPERIMENTAL INVESTIGATION OF HEAT TRANSFER TO CONES IN RAREFIED HYPERSONIC FLOW

Carl T. Berry

Submitted in partial fulfillment of the requirements for the degree of Master of Science in Engineering from Princeton University, 1971.

B407

ACKNOWLEDGEMENT

This research was supported under United States Air Force contracts F 33615-67-C-1065 and F 33615-70-C-1244 and monitored by the Aerospace Research Laboratories of the Office of Aerospace Research, Wright Patterson Air Force Base.

The author would like to express his deep appreciation to the entire staff of the Gas Dynamics Laboratory for their invaluable assistance throughout the course of the present study. The suggestions, advice and encouragement received from Professor S. M. Bogdonoff and Dr. I. E. Vas were most helpful. The laboratory research undertaken would not have been possible without the untiring efforts of technicians I. W. Beecher, Leon Reuter and Alan Patterson. The author is further indebted to Mrs. Jeri Grandy and Mr. D. C. Dynarski for the computer programming, and to Mr. Richard Whitley for maintaining the electrical apparatus. The superb experimental equipment was provided by the Forrestal Machine Shop. Special thanks are extended to Miss Sharon Nuse for typing the manuscript.

ABSTRACT

The present study was an experimental investigation of the surface heat transfer distribution about cones. The study was conducted in the Princeton University hypersonic nitrogen facility covering a wide range of geometries and test conditions in an attempt to evaluate the numerical accuracy, theoretical modeling, and range of applicability of the several theories which are available. Cones, varying from 3° to 30°, with two nose bluntnesses, and lengths from one to eight inches were examined over a range of test conditions, Mach numbers from 16 to 25 and unit Reynolds numbers from 7,000 to 40,000 per inch. The detailed heat transfer distributions, covering the full range of "nose dominated", "merged", and "weak interaction" regimes, were compared with several theoretical prediction techniques. A critical review of the modeling involved in the theories, as compared to the experiments, is presented.

The investigation indicates that the effects of transverse curvature and bluntness have been overestimated in the past. The classical boundary layer theory is shown to predict surface heat transfer quite satisfactorily over most of the range of the study.

TABLE OF CONTENTS

NOMENCLATURE

A	Cross-sectional area of flow
A_w	Cross-sectional area of model skin
$A(\theta_c)$, $B(\theta_c)$	Functions of Mach number, γ , and cone angle (See Ref. 4)
$\hat{A}_o$	$(1/2)\ g_w + (1/6)\ Pr$
C	Constant of proportionality between temperature and viscosity $C_c = \frac{\mu(T_c)}{\mu(T_w)}\ \frac{T_w}{T_c}$; $C_* = \frac{\mu(T_*)}{\mu(T_\infty)}\ \frac{T_\infty}{T_*}$
C_f	Local skin friction coefficient $\equiv \frac{\tau}{(1/2)\rho_\infty u_\infty^2}$
C_p	Constant pressure specific heat; also coefficient of pressure
$C_{H,\infty}$	Heat transfer parameter
C_v	Constant volume specific heat
D_N	Nose Drag
d	Nose diameter of spherical model tip = $2r_o$
d_c	Function of surface temperature, gas properties and free stream conditions (See Ref. 1)
$F_1(k)$	Function of hypersonic similarity parameter (See Ref. 1)
g_w	H_w/H_e
H	Enthalpy
h	Newtonian heat transfer coefficient $h = \dot{q}\ (T_{aw}-T_w)$
K	Hypersonic similarity parameter $K = M_\infty \theta_c$
K_s	Hypersonic similarity parameter $K_s = M_\infty \theta_s$
k	Thermal conductivity; also Newtonian nose drag coefficient (calculated using modified Newtonian, $C_p = C_{p_o} \mathrm{Sin}^2\theta$)

M	Mach number
$\dot{m}$	Mass flow rate
Nu	Nusselt number $\equiv {}^{\alpha x}/_{k}$
n_1	${}^{7g_w}/_{60} + {}^{Pr}/_{36}$
P	Pressure
Pr	Prandtl number $\equiv C_p\mu/k$
P_t	Pitot pressure
$\dot{q}$	Heat flux $[{}^{BTU}/_{ft^2\text{-sec}}]$
Re	Reynolds number
r	$r_o(x) + y \cos \theta_c$
r_o	Radius of spherical model tip
$r_o(x)$	Distance from any point on the body to the centerline axis ($r_o(x) = x \sin \theta_c$)
S	Distance along cone measured from the stagnation point $S = x - r_o [\cot \theta_c - ({}^{\pi}/_{2} - \theta_c)]$
St_c	Stanton number based on invisic cone conditions $St_c = \dfrac{\dot{q}}{\rho_c u_c (H_R - H_w)}$
T	Temperature
T_*	Reference temperature to be used in the determination of the constant of proportionality in the relation: ${}^{\mu}/_{\mu_*} = C_* {}^{T}/_{T_*}$
t	thickness of the blunt leading edge $\equiv 2 r_o \cos \theta_c$; also time
u,v	Velocity in the streamline and normal directions
$\bar{u}$	${}^{u}/_{u_\infty}$
$\bar{V}$	Rarefaction parameter $\equiv M \sqrt{\dfrac{C_*}{Re}}$
w	Exponent relating temperature and viscosity

W — Cone rarefaction parameter

$$W = \frac{\epsilon \rho_\infty u_\infty x \sec \theta_s}{\mu_o} \frac{\mu_o T_*}{\mu_* T_o}$$

$$= \frac{Re_{x,\infty}}{M_\infty^2} \frac{1}{\gamma C_* \cos \theta_c}$$

x,y — Coordinates parallel and perpendicular to the cone surface

$\bar{X}$ — Rarefaction parameter

$$\bar{X} = \frac{\omega_o \tan^4 \theta_c Re_{x,\infty}}{(\gamma-1)^2 C_* M_\infty^2}$$

$Y_b(x)$ — Location of the boundary layer

$Y_E(x)$ — Location of the entropy layer

Y_w — Coordinate of the wall

α — Thermal diffusivity; also experimentally determined flowmeter constant

$\bar{\Gamma}$ — $\dfrac{1}{(1 + \frac{\gamma-1}{2})^{\gamma+1/2(\gamma-1)}}$

γ — Ratio of specific heats $\equiv C_p/C_v$

Δ — $\delta^* \cos \theta$

δ — Boundary layer thickness

δ^* — Boundary layer displacement thickness

ϵ — $\gamma-1/\gamma+1$

ζ — Blunt cone coordinate defined by

$$\zeta \equiv 2 \theta_c^2 S/\sqrt{\epsilon k}\, t$$

θ — Flow deflection angle

θ_c — Cone half angle

θ_s — Shock angle

μ — Viscosity

ρ — Density

τ — Shearing stress $\equiv \mu \left(\frac{\partial u}{\partial y}\right)_{y = 0}$

$\bar{\chi}$ — Hypersonic boundary layer interaction parameter

$$\bar{\chi} = M^3 \sqrt{C_*/Re_x}$$

ψ — Stream function such that $\partial\psi/\partial y = 2\pi r \rho u$

$\bar{\psi}$ — Non-dimensional form of stream function

$$\bar{\psi}^2 \equiv \frac{\psi}{\rho_\infty u_\infty \pi r^2}$$

ω_o, ω_1 — Constants in tangent cone formula

$$\omega_o = \frac{\gamma(\gamma+1)(\gamma+7)}{(\gamma+3)^2}$$

$$\omega_1 = \frac{3\gamma^2 - 7\gamma + 3}{2(\gamma+3)(\gamma+1)}$$

$\bar{\omega}_1$ — $\dfrac{\omega_1}{\omega_o} \dfrac{1}{M_\infty^2 \tan^2 \theta_c}$

Subscripts

w,∞,o — pertaining to wall, freestream, and stagnation conditions respectively

b — refers to spherically blunted cone

c — pertaining to inviscid cone flow

e — pertaining to conditions at the edge of the boundary layer

M — denotes classical Blausius-Mangler solution

s	refers to pointed cone
r	Recovery condition
T	Pertaining to nozzle throat
*	Based on reference temperature T_*

LIST OF FIGURES

I

INTRODUCTION

The present study is an experimental investigation of the heat transfer distribution about cones. With the advent of ultra-high speed flight, an ability to predict local heat transfer distributions in rarefied flows has become increasingly more important to the design engineer. In a broader sense, the present work is part of the continuing program of theoretical and experimental investigation at the Gas Dynamics Laboratory which has been focused on the problem of the interaction between the boundary layer on a slender body and the surrounding hypersonic stream. Although the measurement of surface parameters such as heat transfer, pressure and skin friction are insufficient in themselves to provide a thorough understanding of the problem, it is intended that the present heat transfer investigation will reinforce other studies which have concentrated on the displacement and structure of the shock, the viscous layer profiles and other details of the flow-field development.

The experimental heat transfer results were obtained for slender cones whose half-angles were 3°, 5°, 10°, 15°, 20° and 30°. In addition to the extensive sharp cone studies, blunted cones of the same half-angles (excepting the 3° cone) were investigated to determine the effect of the nose region on the conical afterbody. Tests were conducted over a Mach number range from 16-25 and unit Reynolds numbers from 7,000 to 40,000 per inch.

The flow field over a cone encompasses several fluid mechanical flow regimes ranging from the classical thin boundary layer and inviscid outer flow at large distances downstream to the free molecular flow at the vertex. To evaluate the numerical accuracy and determine the validity of the various theoretical flow models proposed, the results are compared to selected theoretical and experimental

investigations. Primary attention is paid to the fundamental Blausius-Mangler boundary layer solution for the sharp cone, the "weak interaction" formulation of Probstein including transverse curvature[1,2], and the viscous layer analysis of Cheng[3]. The blunt cone results are presented in terms of parameters utilized in the local similarity analysis of Lees[4], and the thin shock layer formulation of Cheng[5].

Becuase flow conditions vary from continuum to free molecular, theoretical modeling for the rarefied conditions of the present experiment is very complicated. The flow over a significant portion of a sharp body in a rarefied gas is characterized by the "merging" of the shock and the boundary layer near the surface. One of the more significant characteristics of the so-called "merged region", which marks the transition from strong or weak interaction to free molecular flow, is the sharply defined thickening of the shock wave. Feik, et.al.[6] have investigated this phenomenon on sharp cones of varying half angle under conditions identical to those of the present study. Using a radiating hot wire to probe the flow-field about the model, Feik determined that for the 5° cone merging begins at a value of $\overline{V}_\infty$ of 0.15 to 0.18, for the 10° cone at a value of $\overline{V}_\infty$ between 0.17 and 0.20, and for the 15° cone at a $\overline{V}_\infty$ of 0.20 and 0.22. At the most rarefied conditions investigated in the present experiment, approximately 2.3" or 27% of the 5° cone was within the merged region, while 1.0" or 33% of the 15° cone experienced merged flow. Although no 3° cone data is available, the merged flow region is most likely of considerable extent. As the cone half angle is increased, it is expected that the boundary layer displacement effect becomes more and more dominant in shortening the merged region. However, extrapolation of Feik's data would lead one to the conclusion that a significant portion of the 20° and 30° cone models were immersed in merged flow during the present investigation.

Experimental measurements of heat transfer at hypersonic speeds and Reynolds numbers low enough to produce "merged flow" are rather limited. Most of these studies have been conducted in shock tunnels or hot shot facilities where run times are extremely short. Shock tunnel heat transfer measurements have been performed on sharp and blunt cones by Wilkinson and Harrington[7] who tested cones of $6\frac{1}{2}^\circ$ and 9° at Mach numbers from 13.5 to 22 and Reynolds numbers from 4,000 to 19,000 per inch. Their sharp cone results followed the viscous layer prediction of Cheng[3] at the lower Reynolds numbers ($W < 50$) and tended toward the transverse curvature predictions of Probstein[2] at the higher Reynolds numbers. Their blunt cone results showed heat transfer as much as 75% greater than had been predicted by Lees[4]. Shock tunnel results at lower Reynolds numbers ($.5 < W < 10$) were obtained by Waldren[8] for 5°, 10° and 20° sharp cones with Mach numbers from 19-24 and Reynolds numbers from 150-4,000 per inch. Waldren's results agreed well with the viscous layer analysis of Cheng. Other shock tunnel data for sharp 9° cones has been obtained by Burke and Dowling[9] and for 5° sharp and blunt cones by Witliff and Wilson[10]. When the various shock tunnel results are compared, they exhibit significant scatter which is as large as 50% even for the higher Reynolds numbers. Griffith and Lewis[11] have obtained hot shot data for 5° spherically blunted cones at Mach numbers near 20 and Reynolds numbers between 8,000 and 15,000 per inch. Their results showed generally good agreement with Lees' laminar theory, and with a slight modification of the parameters suggested by Cheng[5], provided excellent correlation of the data.

A method of avoiding the short run times and the associated thin-film thermometry, which was utilized in the investigations cited above, is the well-known thin-wall technique. This method has been applied successfully at the Gas Dynamics Laboratory for the measurement

of heat transfer rates in its continous facilities. To date there have been very few heat transfer investigations under hypersonic rarefied flow conditions in continuous facilities. Previous measurements under conditions similar to the present study have been limited to those performed by Feik[12] on 5° sharp and blunt cones, by Vas[13] on 10° sharp and blunt cones, and by Gregorek[14] on 10° and 25° blunt cones. The investigation reported herein therefore provides one of the first opportunities for comparison of data from a continuous facility with that taken in the short duration facilities. It also provides the only experimental heat transfer data available for 3° and 30° cones under the present hypersonic flow conditions.

In the following section a brief review of the more pertinent theoretical studies is presented. In section IV comparisons are made between the theoretical predictions and the results which were actually obtained.

II

REVIEW OF THEORETICAL STUDIES

This section contains selected theoretical treatments of heat transfer to pointed and blunt cones in viscous hypersonic flow. Although no attempt is made to survey the extensive literature on the subject, it is hoped that the analyses considered are representative of the fundamental and more easily applied theories of the classical boundary layer, weak interaction, and viscous flow regimes. Comparison of the present experimental results to the theories presented below is postponed until Section IV.

A. Inviscid Cone Solution

Although the present study concerns the viscous phenomenon of heat transfer to cones through a laminar boundary layer, a knowledge of the gas properties of the inviscid flow region between the shock and boundary layer is of considerable importance. In several theoretical studies described below, the heat transfer at the body surface is predicted in terms of the theoretical inviscid flow parameters. The flow field in steady, supersonic flow of an ideal, compressible fluid about a circular cone with an attached shock wave was treated by Taylor and Maccoll[15] in 1933. If the flow is isentropic and irrotational, the second order, non-linear differential equation which describes the flows can be expressed in terms of a single velocity component from which all other variables may be obtained. The so-called Taylor-Maccoll equation can be easily integrated to yield a solution in hypersonic flow if one also adopts the small density assumption, $\rho_\infty/\rho \ll 1$.

Inviscid cone values considered in the present study were taken from tabulations by Sims (personal communication) who had performed the integration in the necessary Mach number range. Inviscid temperature, pressure, and density ratios were assumed functions of M_∞ and θ_c alone, while the theoretical values of Reynolds number at the cone surface was assumed a function of M_∞, θ_c, P_∞, and T_∞.

B. Blausius-Mangler Boundary Layer Solution

The laminar boundary layer on a cone has been treated extensively (For a review of theoretical results see Ref. 16, 17, and 18). The major difficulty in solving the governing differential equation arises from the fact that the fluid properties (μ, k, ρ, c_p) vary with pressure and temperature. As a consequence certain approximations concerning the viscosity-temperature law in the boundary layer must be made or an alternate empirical approach must be taken. A well-known approximate solution with general applicability has been derived by means of a Crocco transformation of the compressible laminar boundary layer equations. Through a change of independent variables, the equations of continuity, motion and energy are reduced to two equations for the unknown enthalpy and shear stress. For the case where the viscosity law ($\mu \sim T^w$) may be considered linear ($w = 1$ or $\rho\mu$ = constant), the differential equation may be transformed to the Blausius equation whose solution yields the result:

$$C_f \sqrt{Re_x} = 0.66412 \qquad \text{II-1}$$

It may also be shown that

$$Nu = 0.332 \sqrt{Re} \sqrt[3]{Pr} \qquad \text{II-2}$$

Since $St \equiv Nu/RePr$

one may write:

$$St = \frac{0.332\ Pr^{-2/3}}{\sqrt{Re_x}} \qquad \text{II-3}$$

This solution for the nondimensional heat transfer to a flat plate

with zero pressure gradient in the boundary layer can be applied to the cone where the Mangler transformation is valid. With the restriction that the boundary layer thickness remain small compared to $r_o(x)$, Mangler has shown that a direct transformation of the boundary-layer equations for axisymmetric flow to those of two-dimensional flow is possible for a perfect gas with constant specific heats. The heat transfer at certain distances along the slant surface from the tip is shown to be $\sqrt{3}$ times the heat transfer at the corresponding flat plate distances from the leading edge.

Thus the Blausius-Mangler solution for heat transfer on a cone may be expressed:

$$St_c = \frac{\sqrt{3}\,(0.332)Pr^{-2/3}}{(Re_{x,c})^{1/2}} \qquad \text{II-4}$$

It has been found that a better estimate of compressible heat transfer may be obtained by a modification of the above equation according to the reference enthalpy method of Eckert[18]. The basic assumption of this empirical method is that heat transfer can be calculated with incompressible flow relations provided all temperature dependent gas properties are evaluated at an appropriate reference enthalpy. According to Eckert, the Blausius-Mangler equation should be altered so that:

$$St_c = \frac{\sqrt{3}\,(0.332)Pr^{-2/3}}{\sqrt{Re_{x,c}}} \sqrt{\frac{\rho_* \mu_*}{\rho_e \mu_e}} \qquad \text{II-5}$$

where the starred quantities are to be calculated at the reference enthalpy. However, instead of using Eckert's reference enthalpy or the wall temperature as a reference as suggested by Chapman and Rubesin[19], one may proceed in an alternative manner. Under the assumptions that

the pressure is constant across the boundary layer and that the body is slender, one may write:

$$\sqrt{\frac{\rho_* \mu_*}{\rho_e \mu_e}} = \sqrt{\frac{\mu_* T_e}{\rho_* \mu_e}} \cong \sqrt{\frac{\mu_* T_\infty}{\mu_\infty T_*}} \qquad \text{II-6}$$

The choice of a reference temperature for this temperature-viscosity relationship may be determined according to the expression proposed by Cheng[5]:

$$T_* = T_o \left[1 + 3(T_w/T_o)\right]/6 \qquad \text{II-7}$$

For a locally similar boundary layer flow around a flat plate Cheng applied the Crocco integral to show that T_* is the average temperature in the boundary layer. Thus one has the modified Blausius-Mangler equation which is applied in the present study:

$$St_c = \sqrt{3}\,(0.332) Pr^{-2/3} \sqrt{\frac{C_*}{Re_{x,c}}} \qquad \text{II-8}$$

where

$$C_* = \frac{\mu_* T_\infty}{\mu_\infty T_*}$$

Although a solution of this form is important because of its wide applicability in the continuum range, it also constitutes the zeroth-order solution for regimes of hypersonic flow where conditions vary considerably from those of the thin boundary layer. The present work verifies that by the choice of an appropriate reference temperature the validity of this solution may extend into gas dynamics regimes where the assumptions of its derivation are inapplicable.

C. Boundary Layer Displacement Effect and Transverse Curvature

1) Weak Interaction

The laminar hypersonic boundary layer on a cone is characterized by a relatively thick curved boundary layer which produces outward deflections on the stream surfaces. This effect can be large enough to significantly change the "effective" shape of the body and perturb the inviscid conical flow field. The perturbations, which result from "induced" pressure changes, are transmitted back into the viscous boundary layer and affect its characteristics. The phenomenon was first recognized by Probstein who authored the definitive work[1] in the the weak interaction regime. Here the influence of the shock wave on the almost uniform flow results in perturbations that are small compared to those upstream where the shock is highly curved.

Probstein's model of the flow consists of a distinct viscous layer of hot gases near the surface separated by a much cooler zone of rotational inviscid flow. The analysis is governed by the Prandtl boundary layer equation neglecting the influence of the immediate nose region and slip effects. The induced pressure field is considered to be specified by the induced flow inclination angle at the edge of the viscous layer. Representation of this pressure field is obtained (in a Taylor series) in powers of the total flow deflection angle, $\frac{d\delta^*}{dx}$. The coefficients of the expansion, which are in the form

$$\frac{1}{p_c/p_\infty}\left[\frac{d\, p/p_\infty}{d\,\theta}\right]_{\theta=\theta_c} \quad \text{and} \quad \frac{1}{p_c/p_\infty}\left[\frac{d^2\, p/p_\infty}{d\,\theta^2}\right]_{\theta=\theta_c} \qquad \text{II-9}$$

may be expressed as functions of γ, M_∞ and the hypersonic similarity parameters K and K_s. It is assumed that the tangent cone approximation and hypersonic similarity apply so that K must be ≥ 1 and $\theta_c \leq 20°$. Under these conditions the value of $\frac{d\delta^*}{dx}$ induced by the viscous flow

is shown to depend on the pressure distribution $p(x,\delta)$. Upon adoption of a linear viscosity relation after the form of Chapman-Rubesin, the induced pressure field is expressed in terms of the interaction parameter $\bar{\chi}_c$. The velocity and temperature profiles of the interaction viscous field may then be expressed asymptotically in ascending powers of $\bar{\chi}_c$. Numerical solutions for the first-order corrections to the velocity and temperature distribution for $Pr = 1$ were obtained by substitution of the asymptotic expressions into the boundary layer equation with the outer boundary condition determined by a term for term matching with the expansion for the external viscous flow. The resultant first-order correction for the boundary layer displacement effect is expressed

$$\frac{q-q_M}{q_M} = [-0.350 + 0.111\,(T_w/T_c) + 0.429\,\gamma - 0.028\,M_c^2][(d_c\,F_1(k)\,\bar{\psi}_c)/\gamma M_c^2] \qquad \text{II-10}$$

The zero order solution is represented by q_M which is the classical Blausius-Mangler solution discussed above.

2) The Transverse Curvature Effect

The laminar boundary layer of an axisymmetric body differs from that of a two-dimensional body because it must spread circumferentially as it grows with distance along the surface. An investigation of this effect by Probstein and Elliot[2] began with the premise that the rate at which the body circumference changes with length is the axisymmetric geometrical factor which determines the characteristics of the viscous layer. It was found that the transverse curvature effect is characterized by the parameter $\Delta/r_o(x)$, which is essentially the ratio of boundary-layer thickness to body radius. For an insulated cone of half-angle θ_c

in supersonic flow:

$$(\Delta/r_o(x))_M = \frac{0.994 + 0.275\, M_c^2}{\tan \theta_c} \sqrt{\left(\frac{C}{Re_x}\right)_c} \qquad \text{II-11}$$

This expression is intended as a criterion for determining the extent of the nose region where $\Delta/r_o(x) \gg 1$ and the downstream region where $\Delta/r_o(x)$ is on the order of or less than unity.

Probstein and Elliot treat the transverse curvature effect in the region where $\Delta/r_o(x) < 1$. First, the Busemann and Crocco integrals of the two-dimensional energy equation for $Pr = 1$ are shown to be valid for axisymmetric flow in which transverse curvature effects are considered. Then the boundary-layer equations are reduced to an almost two-dimensional form through a modified Mangler transformation, and a solution is obtained for the region where $\Delta/r_o(x) < 1$. For the cone with zero pressure gradient in a perfect gas having constant specific heats and a Prandtl number of unity, the heat flux may be written:

$$\frac{q-q_M}{q_M} = [0.517 + 0.913\,(T_w/T_c) + 0.121\,(\gamma-1)M_c^2] \left[\sqrt{3}\tan\theta_c \sqrt{\left(\frac{C}{Re_x}\right)_c}\right] \qquad \text{II-12}$$

This equation is also expressed in terms of the classical boundary-layer results, q_M, which one obtains using the Mangler formulation.

It is important to note that the corrections obtained for the boundary-layer displacement effect were also in inverse powers of $(Re_{x,c})^{1/2}$. Probstein recognized that the principle of linear superposition applies and that the transverse curvature and induced pressure effects are directly additive. By combining the corresponding corrections, Equations II-10 and II-12, the total heat transfer may be expressed as

$$St_c = \sqrt{3}\,(0.332)\,Pr^{-2/3}\sqrt{\frac{C}{Re_{x\,c}}}\;\{1 + [-0.350 + 0.111\,(\frac{T_w}{T_c}) + (0.429\,\gamma - 0.028)M_c^2][d_c\,F_1(k)\,\bar{\psi}_c/\gamma M_c^2] + [0.517 + 0.913(T_w/T_c) + 0.121(\gamma-1)M_c^2]\,[\frac{1}{\sqrt{3}\tan\theta_c}\sqrt{\frac{C}{Re_{x\,c}}}]\}$$ II-13

The transverse curvature correction is larger than that for induced pressure over the entire cone half-angle range. For the present test conditions and the 3° cone the transverse curvature correction is about 50% larger while for the 20° cone it is about 20% larger.

D. Solomon-Loeb Pohlhausen Solution for Hypersonic Boundary Layers

Since the publication of Probstein's papers on the induced pressure and transverse curvature effects, several approaches to the same or similar problems have been treated by the Pohlhausen method[20]. Application of the Pohlhausen technique involves an integration of the boundary-layer momentum equation to yield an ordinary differential equation for the variation of one free parameter along the body surface. The solution of this equation completely specifies the approximate velocity profile at each point along the body surface, and all flow properties of interest may be determined.

A recent Pohlhausen solution for conical flows has been obtained by Solomon and Loeb[21] who consider the same problem as Probstein's: the approximate analysis of the self-induced pressure on slender bodies in the presence of transverse curvature effects. The only major difference in the formulation of the problem is that Probstein assumes hypersonic similarity and procedes by the series expansion method, while the authors of the more recent study utilize the

Pohlhausen technique. Restrictions on the analysis and the other assumptions are very similar (See Sec. C). The flow field is assumed to consist of two parts: A viscous boundary layer adjacent to the body surface and a purely inviscid flow between the boundary layer and the shock. In the boundary layer Pr and C_p are considered constant and a linear viscosity-temperature law is assumed. The inviscid Mach number, M_e, is considered large enough so that $H_e/h_e \gg 1$. The latter assumption allows the authors to adopt the hypersonic approximation which essentially specifies that $u_e^2 = 2H_e$.

The governing momentum integral equation obtained by the Pohlhausen technique is convenient because the inviscid flow enters only through a variation of P_e. The resultant pressure dependence suggests the adoption of an empirical expression for the inviscid pressure field in order that the induced pressure problem may be studied in conjunction with the transverse curvature effect. This induced pressure problem can only be solved where the boundary layer and the inviscid flow are solved simultaneously. Thus, the Pohlhausen solution of the boundary layer is constructed to allow for a significant alteration in the inviscid flow field due to the displacement of the boundary layer. To solve for the inviscid flow field, an "effective body" is assumed to exist with the same inviscid field as the original body with all viscous effects neglected. The surface pressure on the "effective body" is described by a tangent cone formula in the following form:

$$P_e/P_\infty = \omega_o K^2 + \omega_1 \qquad \text{where} \qquad K = M_\infty \tan\theta \qquad \text{II-14}$$

In this manner the local inviscid pressure on the "surface of the effective body" is related to the undisturbed flow ahead of the body through conical flow theory, but using the local surface inclination as the effective cone angle.

Solutions of the governing momentum integral equation with the inviscid pressure so defined are obtained by Solomon-Loeb for the limiting cases of very small and very large transverse curvature effects. The limiting cases are defined in terms of a variable which contains all of the relevant parameters:

$$\bar{\underline{X}} = \frac{\omega_o \tan^4\theta_c \, Re_{x,\infty}}{(\gamma-1)^2 C_* M_\infty^2} \qquad \text{II-15}$$

Since the transverse curvature effect increases with decreasing Reynolds numbers, increasing Mach number, and decreasing semi-vertex angle, it is quite natural that the heat transfer solution for large transverse curvature be expressed as a limiting solution as $\bar{\underline{X}} \to 0$. Neglecting terms of $O([\log\log \frac{1}{\bar{\underline{X}}}]/\log \bar{\underline{X}})$ the heat transfer may be expressed:

$$C_{H,\infty} = \frac{(\frac{2\,\omega_o \hat{A}_o}{\gamma-1}) \tan^3\theta_c \, \frac{H_\infty}{H_e Pr} (\frac{H_e Pr - H_w}{H_o - H_w})}{\bar{\underline{X}} \log \frac{1}{\bar{\underline{X}}}} \quad \text{as } \bar{\underline{X}} \to 0 \qquad \text{II-16}$$

For the opposite limit of small transverse curvature effects, the heat transfer solution is given in decreasing negative powers of $\bar{\underline{X}}$ and the classical boundary layer solution is approached as $\bar{\underline{X}} \to \infty$ For this case the equation may be written

$$C_{H,\infty} = (\frac{H_e Pr - H_w}{H_{o,\infty} - H_w}) \frac{\omega_o \tan^3\theta_c}{Pr\,\gamma-1)} \{\frac{\sqrt{1+\bar{\omega}_1}}{2} \frac{1}{\sqrt{\bar{\underline{X}}}} +$$

$$+ \ {}^2/_5 (\frac{1}{1+\bar{\omega}_1}) [3 (1+\bar{\omega}_1)\hat{n}_1 + \qquad \text{II-17}$$

$$\frac{\hat{A}_o}{2} (1 + \frac{3(\gamma-1)}{2\gamma}\hat{A}_o)] \frac{1}{\bar{\underline{X}}} \} \quad \text{as } \bar{\underline{X}} \to \infty$$

E. The Viscous-Layer Regime as Analysed by Cheng

Due to the design alterations in the 20° and 30° cones, it was possible to obtain heat transfer data at stations in the vicinity of the leading edge (0.1 inch $\leq$ x) of these models. For the lower Reynolds number conditions of the present study, the flow about the forward regions of the models denoted above may be classified as belonging to the "viscous-layer regime", because here the viscous layer becomes the dominant fraction of the shock layer. Departures from the predictions of thin boundary-layer concept in this flow regime become more and more evident as rarefaction is increased (See Ref. 8). To the author's knowledge, the only solution applicable to flows over pointed cones where the shock layer is fully viscous has been formulated by Cheng[3]. The outstanding features of the portions of Cheng's analysis which are applicable to the present investigation are discussed briefly below.

According to Cheng's flow model for the viscous layer regime, the flow field around a body in rarefied flow can be divided conveniently into two regions: the shock layer and the shock-transition zones. The compression ratio across the shock-transition zone is assumed to be high, and both regions are assumed to be thin in comparison to a typical body dimension. The analysis begins with a consideration of the Navier-Stokes equations governing compressible, heat conducting flow. By neglecting transverse curvature and retaining only the highest order normal derivatives in the transport terms, Cheng obtains a parabolic system of equations similar to the boundary-layer equations of compressible flow. In the formulation of the problem for the thin shock layer the non-slip boundary condition is adopted at the body surface. This boundary condition is justified by a manipulation of the momentum and energy equations of the Navier-Stokes equations to show that the phenomenon of velocity slip and temperature jump can

be neglected. Other assumptions of the analysis involve the neglect of transverse curvature, the boundary layer displacement effect and shock curvature in comparison to the more important slip-like velocity and enthalpy changes across the shock. The validity of the analysis is limited to thin shock layers over highly cooled surfaces and non-slender cones where $\delta/r_o \ll 1$. The gas is assumed to be perfect with constant specific heats and unit Prandtl number. Under this framework and with the adoption of a linear viscosity law, the analysis is reduced to the solution of a single parabolic differential equation governing the velocity:

$$W \frac{\partial(\bar{u}^2/2)}{\partial W} = 2 \bar{\psi} \frac{\partial(\bar{u}^2/2)}{\partial \bar{\psi}} + 4 \bar{u}/W \frac{\partial^2(\bar{u}^2/2)}{\partial \bar{\psi}^2} \qquad \text{II-18}$$

with the boundary conditions ($\bar{\psi} = 1$ at shock):

$$\bar{u}(0) = 0$$

$$\bar{u}(1) = 1 + \frac{2}{W} \left[\frac{\partial(\bar{u}^2/2)}{\partial \bar{\psi}} \right]_{\bar{\psi} = 1} \qquad \text{II-19}$$

Since the equation is of the parabolic type, forward integration is possible and a nonsimilar solution may be obtained by the method of finite differences. Comparison of the resultant solution to the Blausius profile reveals close agreement down to a value of $W \simeq 3$, even though the shock layer is fully viscous at that point. The comparison reveals that departure from the predicted values of heat transfer by the thin boundary layer theory should first occur at $W \cong 3$ and become significant at $W \cong 1$.

It is important to note that the effects of gas rarefaction and surface incidence are all contained in, and can therefore be correlated

by, the variable W .

$$W = \frac{\epsilon \rho_\infty u_\infty x}{\mu_o} \left(\frac{\mu_o T_*}{\mu_* T_o}\right) \sec \theta_s$$

$$= \frac{Re_{x,\infty}}{M_\infty^2} \frac{1}{\gamma C_* \cos \theta_s} \qquad \text{II-20}$$

Cheng presents his heat transfer prediction in terms of the parameters:

$$C_{H,\infty}/\sin \theta_s \quad \text{vs} \quad W \qquad \text{II-21}$$

The numerical solution presented is valid in the region $0 < W < 10$, and it approaches the classical free-molecular and boundary layer results at the extremes of the region. The solution first begins to depart from the classical boundary layer theory at $W \simeq 3$ and $C_{H,\infty}$ approaches the value of $\sin \theta_s$ as $W \to 0$ as required by free-molecular-flow theory for unit accommodation coefficients.

Cheng's formulation is especially valuable in the analysis of the present data because all of the experimental variables are contained in one convenient correlation parameter.

F. Lees' Local Similarity Analysis

The concept of assuming a local similarity in the boundary layer as a means of estimating heat transfer to blunt bodies at high speeds was first proposed by Lester Lees[4]. By using the Levy transformation to transform the momentum and energy equations into a more convenient "low speed" form, he obtained locally similar solutions to the boundary layer equations. Lees observed that the enthalpy distribution in the boundary layer is rather insensitive to pressure gradient. In effect he found that the nondimensionalized enthalpy gradient at the surface is represented very accurately by the classical zero-pressure gradient value, and that the surface heat transfer rate can be obtained

in terms of the pressure distribution.

Applications of the result were obtained for the special cases of the hemisphere and the right circular cone capped by a spherical segment. The modified Newtonian pressure distribution in the form:

$$p/p_o = \cos^2\theta \ (1 + \gamma_\infty M_\infty^2) \sin^2\theta \qquad \text{II-22}$$

was adopted as a means of calculating the heat transfer distributions.

For the hemisphere and the leading edge of the spherically blunted cone Lees' result may be written:

$$\frac{q_w}{(q_w)_o} = \frac{(1/2)\theta \sin\theta \ [\cos^2\theta + (1/\gamma_\infty M_\infty^2)\sin^2\theta]}{\int_o^\infty \sin^2\theta \ [\cos^2\theta + (1/\gamma_\infty M_\infty^2) \sin^2\theta]d\theta} \qquad \text{II-23}$$

The modified Newtonian pressure distribution is also assumed for the conical skirt where all physical quantities are regarded as constant. The result for the heat transfer distribution for $x/r_o \geq \cot\theta_c$ may be written

$$\frac{q_w}{(q_w)_o} = A(\theta_c) \ \frac{x/r_o}{[B(\theta_c) + (x/r_o)^3]^{1/2}} \qquad \text{II-24}$$

$A(\theta_c)$ and $B(\theta_c)$ are functions of γ, M_∞ and θ_c (Ref. 4). At the junction of the nose and conical skirt the two expressions for $q_w/(q_w)_o$ are identical. Lees' result predicts for blunted cones a heat transfer rate that is smaller than that of an equivalent sharp cone for several nose radii aft of the nose - skirt junction.

G. Combined Leading Edge Bluntness and Boundary Layer Displacement - Cheng's Thin Shock Layer Theory

Within the formalism of the classical boundary layer theory and the hypersonic small disturbance theory, Cheng[3] has theoretically

treated hypersonic flows over thin bodies subject to the combined effect of leading edge bluntness and boundary layer displacement for two dimensional and axisymmetric flows. Although separate treatments of either boundary-layer displacement or bluntness alone received considerable attention during the 1950's, Cheng[5] was the first to attack the combined problem satisfactorily. His approach is characterized by two basic concepts: a local similarity in the boundary layer and a detached shock in the outer inviscid flow. His basic flow model consists of a low density entropy layer situated between the laminar boundary layer and the shock layer. This inviscid region termed the "entropy layer" is so designated because it consists of gas particles which have come through the stronger, forward portion of the shock. The terminology is appropriate since the specific entropy of these particles is much higher than that of particles passing through the comparatively straight shock downstream of the nose region and farther away from the body.

The domain of validity of Cheng's formulation is limited by several restrictions which govern the accuracy of the analysis in the inviscid-flow regime and the boundary layer. Underlying the analysis are the requirements that $1/(M^2\theta_c^2)$ and $\epsilon = \gamma-1/\gamma+1$ be sufficiently small in comparison to unity to permit treatment by the shock layer concept. (For Mach numbers and flow deflection angles such that $1/M^2\theta_c^2 \ll 1$ a strong shock exists). Through a transformation of the boundary layer equations, the assumption that ϵ be small is shown to be essential in order to neglect the normal pressure gradient across the boundary layer. The Cheng formulation is ideally applied in the limit of $\gamma \to 1$ because the direct effect of pressure gradient is at most of order ϵ. However, it is argued that the formulation is valid for small ϵ since the leading approximation of the solution to the transformed boundary layer equations

is independent of ϵ and is governed by the Blausius equation.

Cheng's analysis is further restricted by the simplifying assumption that $u_e \approx u_\infty$ at the outer edge of the boundary layer and within the entropy layer as well. He shows that the error in this assumption may be expressed:

$$\left|\frac{u_e - u_\infty}{u_\infty}\right| \leq (1/2)\theta_c^{2(\gamma-1)/\gamma} \qquad \text{II-25}$$

Cheng insists that this quantity be negligible in comparison to unity, but at the same time he recognizes that θ_c must not be so small that the strong shock assumption is violated. Satisfaction of the former restriction on θ_c not only insures that the perturbation velocities will be small, but also that the analysis of the entropy layer can be based upon the fact that the prevailing density is much lower than that of the free stream. As an immediate consequence the pressure variation across the entropy layer can be shown to be negligible. In fact he demonstrates that the fields of pressure and velocity, as well as the shock locations can be consistently determined under the restriction he sets forth.

On the formulation of the differential equation for the location of the entropy layer, $Y_E(x)$, Cheng considers the inner edge of this layer as an equivalent body surface to account for the displacement effect. The local pressure at the outer edge of the entropy layer and hence in the complete region $Y_b < y < Y_e$ can be calculated from the Busemann formula when the local shape of the outer edge of the entropy layer is determined:

$$P_b = \gamma_\infty P_\infty M_\infty^2 [Y_e Y_e']' \qquad \text{II-26}$$

Since $u(x) \approx u_\infty$ everywhere in the entropy layer, the continuity and

momentum equations are integrated twice to yield

$$[Y_e - Y_b]^{\gamma} \; P_b = \text{constant} \qquad \text{II-27}$$

A combination of the two equations yields the necessary ordinary differential equation for the entropy layer (assuming $\gamma \to 1$):

$$[Y_e - Y_b][Y_e \; Y_e']' = \text{constant} = 1/2\sqrt{\epsilon k}\; t \qquad \text{II-28}$$

Where the constant on the right hand side may be obtained from an integral of the momentum equation over a cross section normal to the free-stream direction. Since $Y_b = Y_w + \delta^*$, it is clear that the manner in which the boundary shock and the entropy layers interact is contained in the ordinary differential equation given above.

For the axisymmetric case the necessary differential equation for $Y_e(x)$ may be expressed:

$$Z^Z - \zeta^2 \; (ZZ')' = 2 \qquad \text{II-29}$$

where

$$Z = 2\,\theta_c\, Y_e \,/\, \sqrt{\epsilon k}\; t \qquad \text{II-30}$$

$$\zeta = 2\,\theta_c{}^2\, S \,/\sqrt{\epsilon k}\; t \qquad \text{II-31}$$

$$k = \frac{D_N}{(1/2)\rho_\infty \; u_\infty{}^2(\pi t^2/4)} \qquad \text{II-32}$$

Although there results a power law relationship for Z in the solution for small ζ (near the leading edge) the asymptotic behavior of this equation for large ζ yields a solution which is expressed

in terms of Bessel functions of the first and second kind. As a result the boundary layer pressure dependence on axial location, $P(\zeta)$, is characterized by the exponentially decaying, oscillatory behavior of the Bessel functions. The implication of this result in regard to the theoretical heat transfer predictions is obvious. To the leading approximation for small ϵ, Cheng shows that the heat transfer may be expressed explicitly as a function of pressure alone.

$$C_{H,\infty} M^3 \approx \bar{\chi}_t \frac{P/P_\infty}{\sqrt{\int_0^s P/P_\infty \frac{dS}{L}}} \qquad \text{II-33}$$

As a consequence of this pressure dependence a correspondingly oscillatory behavior is manifested in the predicted heat transfer distribution.

For the blunt cone Cheng suggests correlating the heat transfer dependence in terms of the parameters.

$$M_\infty^2 (\epsilon k)^{1/4} C_{H,\infty}/\theta_c^2 \bar{\chi}_t \quad \text{vs} \quad \frac{\theta_c^2 S}{\sqrt{\epsilon k}\, t} \qquad \text{II-34}$$

The nature of the oscillatory solution may be observed in Figs. 22-26. A rapid changeover to oscillatory behavior is predicted for the vicinity of

$$\frac{\theta_c^2 S}{\sqrt{\epsilon k}\, t} = 1 \qquad \text{II-35}$$

Cheng suggests that the oscillation is attributable to a repeated reflection or skipping of the reattaching shock layer as it reaches the vicinity of the surface of the conical afterbody. However, he concedes that the phenomenon of glancing reimpingement of the shock layer may be substantially altered by higher order calculation in ϵ.

In spite of the fact that the several essentially restrictive assumptions of the analysis can nver be absolutely satisfied, there

appears to be a fairly extensive range of hypersonic flows where such a "thin shock layer" theory should apply. The geometries and flow conditions of the present investigation were such that most restrictions were well satisfied although the 5° and 30° cone angles approach the lower and upper limits required of θ_c .

III

THE EXPERIMENTAL METHOD

A. Introduction

The experimental method used to determine the local convective heat transfer to the conical bodies was the well-known transient "thin-wall" technique. Sharp and blunt thin-skinned conical shells, which varied in half angle from 3° to 30°, were installed with copper constantan thermocouples and tested in the hot nitrogen facilities. From the simple heat balance for an element of model skin it can be shown that determination of the temperature rise with time is necessary and sufficient for computing the local heat transfer coefficients at the model wall. The models, initially maintained at a low isothermal wall temperature ($T_w/T_o = 0.14$), were suddenly exposed to the free stream when a pneumatically operated shield was removed. The temperature vs. time history of the models was recorded on an oscillograph which monitored the voltage level of each thermocouple. The temperature data was differentiated and digitized auto-mechanically in order that repetitive calculations could be accomplished by computer.

B. Facilities and Test Conditions

Two nearly identical hypersonic wind tunnels were used for the present investigation. The majority of the work was completed in the Princeton Hypersonic Tunnel N-3 while the Hypersonic Tunnel N-5 was utilized for a small portion of the program. Both tunnels are blow down facilities with maximum running times of 25 minutes. Since the newer N-5 tunnel is an almost exact duplicate of the N-3 facility, separate descriptions are redundant (Fig. 1). Only those details having a direct bearing on the present investigation will be considered, since a comprehensive description of the N-3 facility is given by Vas and Koppenwallner[22].

The working gas is high purity nitrogen (contamination of oxygen less than 8 parts per million) which is heated by a graphite resistance element[23] to stagnation temperatures sufficiently high to yield a static temperature throughout the expansion which precludes the possibility of condensation. A wide range of flow conditions is achieved by alternately exmploying one of two conical nozzles which expand the flow into the six inch diameter test section. The higher range of Reynolds numbers from 17,000-41,000/in. are obtained with the 6° half-angle conical nozzle at stagnation pressures from 2,000 to 4,000 psia and stagnation temperatures of 2,000° K and 1,700° K respectively. Corresponding Mach numbers range from 17 to 19. Lower Reynolds numbers from 7,000 to 14,000/in. at Mach numbers from 23 to 27 can be obtained when the expansion is accomplished by the 10° half-angle conical nozzle. The stagnation pressures required were 2,000, 3,000, and 5,000 psia at a constant stagnation temperature of 2,000° K . The free stream parameters corresponding to the five stagnation conditions at which each model was tested is presented in Table I.

At 4,000 psia the diameter of the usable inviscid core of the wind tunnels is about 4" at the nozzle exit, decreasing to 2" at about twelve inches downstream. All models were aligned to the tunnel centerline with their tips located a nominal 4" from the nozzle exit. This positioning insured that the entire conical surface was well within the inviscid core. The reasonable quality of the core section at the station of the model tips is shown in Figure 2. Since the conical nozzles are only partially "contoured" by the growth of the tunnel boundary layer, a slight expansion process continues into the test section resulting in a Mach number gradient along the centerline of 0.3 per inch for the higher Mach number range. Corrections for this gradient are incorporated into the computerized data reduction program.

In the interpretation of heat transfer data an accurate determination of the thermodynamic state of the free stream gas is of critical importance, because it is both customary and convenient to normalize local heat flux by free stream conditions inferred from the stagnation conditions and measured pitot pressure. In addition the nondimensionalized heat flux data is usually correlated by parameters which are strong functions of $Re_{x,\infty}$, the Reynolds number based on free stream conditions. Consequently any error in measuring the stagnation conditions can be compounded when results are compared to theory. Some attention should therefore be given to the assumptions and measured quantities used to infer these free stream conditions in the hot nitrogen facilities.

Although dissociation effects are of no concern in the N-3 facility, the thermodynamic properties of the gas must be specified with attention paid to the vibrational energy of the diatomic gas as well as the translational and rotational constituents of the total thermal energy. Consideration of the former demands that the freezing temperature for the vibrational mode of the gas be determined. Vas and Koppenwallner[22] have shown that a freezing of the vibrational energy occurs so close to the throat that the assumption that the flow is vibrationally frozen throughout the expansion results in only 0.5% error in Mach number. Acceptance of this approximation results in a considerable simplification, the number of necessary parameters being reduced from four to three; P_o , T_o , and P_t . With knowledge of these three quantities the thermodynamic system is completely specified under the vibrationally frozen assumption and all free stream quantities of interest can be calculated.

Impact pressures are measured using a variable reluctance transducer calibrated with a silicon (high vacuum) oil manometer, while the stagnation pressure, P_o , is measured with a precision

Heise bourdon gage. Since the elevated temperature of a highly pressurized gas is difficult to measure accurately with thermocouples, the stagnation temperature is inferred from the mass flow rate of the incoming gas through a Potter turbine flowmeter. Details of this method should be scrutinized since Stanton number and Reynolds number are functions of stagnation temperature.

Inference of the stagnation temperature from the mass flow rate is justified if a number of assumptions are valid. If along the gas inlet line at any point of interest (including the stagnation chamber and nozzle orifice) one can consider the flow to be isentropic and sufficiently uniform to warrant the one-dimensional assumption, the same mass flow must exist at any station. For steady flow:

$$\dot{m} = \rho u A = \text{constant} \qquad \text{III-1}$$

Inserting

$$\rho = P/RT \quad \text{and} \quad u = M\sqrt{\gamma RT}$$

One may write:

$$\dot{m} = (P/RT)M \sqrt{\gamma RT} A \qquad \text{III-2}$$

Utilizing the isentropic relationships for total temperature and pressure:

$$T_o/T = 1 + \frac{\gamma-1}{2} M^2 \qquad \text{III-3}$$

$$P_o/P = \{(1 + \frac{\gamma-1}{2})M^2\}^{\gamma/(\gamma-1)} \qquad \text{III-4}$$

One obtains:

$$\dot{m} = \sqrt{\gamma/R}\ \frac{P_o A}{\sqrt{T_o}}\ \left\{\frac{M}{\left(1 + \frac{\gamma-1}{2} M^2\right)^{(\gamma+1)/(\gamma-1)}}\right\} \qquad \text{III-5}$$

Imposing the sonic condition at the throat and denoting

$$\bar{\Gamma} = \frac{1}{\left(1 + \frac{\gamma-1}{2}\right)^{(\gamma+1)/2(\gamma-1)}} \qquad \text{III-6}$$

One may write finally:

$$\dot{m} = \frac{\bar{\Gamma} P_o A_T}{\sqrt{T_o}}\ \sqrt{\gamma/R} \qquad \text{III-7}$$

The functional dependence of $\bar{\Gamma}$ on pressure has been investigated and is presented by Vas and Harvey[23]. Knowing $\bar{\Gamma}$; the mass flow rate, $\dot{m}$; the stagnation pressure, P_o ; and the throat size, A_T ; the stagnation temperature can be calculated.

A Potter turbine flowmeter was used to measure the mass flow. Although the turbine flowmeter is ideally a volumetric flowmeter, it becomes a mass flowmeter upon specification of pressure and temperature of the gas in the meter.

The output of the flowmeter is related to the mass flow as follows:

$$\omega = \dot{m}/\alpha\rho \qquad \text{III-8}$$

where:

ω = frequency of turbine flowmeter (cps)

ρ = density of gas in flowmeter based on T_{FM} , P_{FM}

α = experimentally determined flowmeter constant

The output, ω , is displayed on a C.M.C. Universal Counter Timer. The density of the gas in the flowmeter was determined from data presented by Michels, et.al.[24] which accounted for the non-ideal behavior of nitrogen under high pressures.

Calibration of the flowmeter over the pressure range from 1,500 to 5,000 psia allowed the determination of the constant, α . It was found that the Potter meters used were not true volumetric flowmeters but that α decreased with increasing stagnation pressures for each of the three meters used. Each meter showed a decrease of approximately 7% in α over the pressure range. Since an error of this magnitude in flowmeter count would have resulted in a stagnation temperature error of about 15%, accurate values of α at each stagnation pressure were determined to within an accuracy of 1%, and $\alpha = \alpha\,(P_{FM})$ was inserted into the flowmeter equation:

$$\omega = \frac{\bar{\Gamma}\, P_o A^*}{\sqrt{T_o}} \sqrt{\gamma/R}\ \frac{1}{\alpha(P_{FM})\rho} \qquad \text{III-9}$$

From the above equation working curves were constructed of T_o vs. ω for varying inlet gas temperatures, different stagnation pressures and throat diameters. Although the calibration mentioned above was performed at room temperature, it was further assumed that the throat boundary layer during tunnel operation is infinitesimally small, since the Reynolds number based on orifice conditions is so large.

The scatter in the "cold flow" calibration used to determine effective throat diameter (knowing P_o , T_o , and ω) limits one to an uncertainty in T_o of $\pm$ 50°K at T_o = 2,000°K. A more serious inaccuracy in this method of inferring stagnation temperature arises from the deposition in the nozzle orifice of carbon particles loosened from the graphite heater element. Over the period of an

individual tunnel test the effective throat diameter sometimes changes several ten-thousanths of an inch from the nominal 0.0320 orifice employed with the 10° conical nozzle. Since the stagnation temperature varies as the square of the throat diameter, data was discarded when changes of this order occurred. However, minor fluctuations in throat error were unavoidable. The resultant variations could be detected by a reference thermocouple on each model which monitored heating rates at a particular location during each exposure to the flow. When the tunnels operate at the lowest stagnation pressure (2,000 psia), carbon tends to deposit gradually in the orifice decreasing its area. For a constant flowmeter count there results a continually decreasing stagnation temperature even though the power consumption of the resistance heater remains constant. Conversely, at higher stagnation pressures the previously deposited carbon tends to blow downstream with the corresponding increase in throat area causing an associated increase in stagnation temperature. The stagnation temperature is therefore uncertain to $\pm$ 100°K , or $\pm$ 5% . An improvement in the construction of the graphite resistance element would considerably reduce scatter in future data to be obtained in the facilities. Implications and further observations concerning the problems mentioned above will be considered in the error analysis, Section III-G.

C. The Experimental Models

Typical blunt and sharp heat transfer models are shown in Figures 3 and 4. Each model consists of a right-circular conical shell capped by a spherical segment. The "sharp" models were designed with a spherical cap only 0.004" in diameter. Since this dimension is on the same order as the mean free path, one can consider a mathematically sharp cone. The "blunt" cones are constructed with a spherical segment whose diameter is 0.225", approximately 100 mean

free paths.

The conical shells were constructed of electroformed nickel and instrumented with ten to twenty 0.005" copper-constantan thermocouples which were peened tightly into place at fairly uniform intervals along the conical surface. No attempt was made to describe the heat transfer to the cylindrical portion of the model, although at least two thermocouples were installed there so that a tunnel stall or conduction from the sting could be detected.

As a first step in the construction of a model, a plexiglass mandrel was smoothly machined to the required inner diameter of the cone. Nickel was then electroplated to a thickness of about 0.020". From this rough surface a smooth conical shell was machined to a uniform thickness of 0.010" and to the desired apex angle. The model was then instrumented with the copper-constantan thermocouples. Most of the thermocouples were placed along a particular ray of the cone. However, four thermocouples were placed in the surface at 90° intervals of arc in order that it could be verified that the angle of yaw in the wind tunnel test section was as close as possible to zero degrees. The cylindrical afterbody of the cone was then attached to a water-cooled holder which provided two leadout tubes for the thermocouples, an inlet tube for the nitrogen cooling gas, as well as a means for sting mounting the model in the wind tunnel.

Initially the heat transfer models were designed with a $1\frac{1}{2}$" base diameter and interchangeable tips. Two of these models, denoted as "Type I", are depicted in Figure 3. Type I models were designed with interchangeable tips for convenience and economy. A single model of this type would suffice both as a "sharp" and a "blunt" model with a single tunnel installation, and conversion could be accomplished in minutes without affecting the alignment of the model to the flow. The versatility of the design is of significance in that the effects

of bluntness could not be obscured by a variance in model skin thickness or a change in tunnel alignment resulting from the installation of a separate sharp or blunt model of the same apex angle.

Upon the reduction of the data from the first Type I model to be tested, a disadvantage of this construction was revealed which led to a modification in the design of several models. The solid steel tip and its mount inside the nickel shell constituted a substantial heat sink which resulted in considerable conduction errors in the tip region. As a result a significant portion of the data from the more rarefied region of the shell was discarded.

The conduction to the solid tip and the necessity of reducing the model base diameter resulted in the construction of the Type II models. Tests of dummy models proved that 20° and 30° cones could be "started" successfully at the lowest desired stagnation pressure if the base diameters of the models were decreased to 1 inch. Since the conical shell of a 30° half-angle cone with a base diameter of only 1" is itself only 1" long, the initial Type I design would have resulted in a model severely affected by conduction along its entire length. Consequently, new 20° sharp, 20° blunt, 30° sharp and 30° blunt cones were designed with 0.010" skin thickness including the region of the tip. The plexiglass mandrels were ground to exacting specifications and meticulous machining of the electroplated nickel was required to insure uniformity of the wall thickness both along the conical shell and around the spherical cap. The design permitted the installation of thermocouples close to the tip which were only slightly affected by conduction.

No Type II 3°, 5°, or 15° models were constructed since these models were long enough that the middle and after portions of the conical shells were virtually unaffected by the solid tips. The fact that identical results for the after portions of the cone are obtained

using Type I and Type II models has been verified experimentally by Vas[13]. Refer to Table II for the type and relevant dimensions of the various conical models.

D. Mounting and Alignment

The cone models were supported on the rear of the cylindrical afterbody by means of a cylindrical holder which was attached to a copper sleeve fitted to the model. A water cooled strut, which could be adjusted for pitch and yaw provided support for the holder. The models were aligned as closely as possible to the tunnel centerline, but it was physically impossible to view the model by telescope during tunnel operation (See Figs. 5 and 6). The only check on the flow angularity was provided by the four circumferentially spaced thermocouples located at 90° intervals of arc midway to the cone base. If data reduction subsequent to the test revealed equal heating rates, the model was considered to be properly aligned. If more than 10% variation was observed, the model was realigned. From experience it was found that a negative angle of attack of ten minutes provided near optimum alignment.

E. The Transient Thin-Wall Technique

The local heat transfer coefficient for a thin-skinned body can be determined from a simple algebraic equation if certain restrictions are satisfied. For proper application of the thin-wall technique the time derivative of temperature within the skin normal to the surface must be constant, conduction along the surface of the model must be negligible compared to the heat input, and radiation losses are required to be small. Under such conditions the following simple heat balance for an element of skin may be written:

$$\dot{q} = \frac{h}{T_{aw}-T_w} = \rho_w c_w \left(\frac{dV}{dA}\right)_w \left(\frac{\partial T}{\partial t}\right)_{w \atop (t=0)} \qquad \text{III-10}$$

The term $(dV/dA)_w$ is determined from the model geometry and is approximately equal to the wall thickness for a cone, while the density and specific heat of the wall material are practically constant over the small temperature range of the present experiment. Since the model walls were cooled to an isothermal temperature of approximately 32° F and the highest temperatures used for data purposes was 80° F the assumption of constant wall properties is quite sufficient for the present experiments.

An important assumption in the derivation of the local heat balance for an element of thin skin is that the temperature normal to the surface be uniform, because satisfaction of this criterion assures the uniformity of $\partial T/\partial t$. Manos and Taylor[25] point out that $(\alpha t)^{\frac{1}{2}}$, the distance characteristic of thermal diffusion must be much greater than the skin thickness. More specifically they have shown that if:

$$\frac{\pi^2 \alpha t}{\delta^2} \gg 1 \qquad \text{III-11}$$

then the time derivative of skin temperature in the direction normal to the surface is constant. Inserting the values of $\alpha = 1.65 \times 10^{-5}$ $ft^2/sec.$, $\delta = 0.000833$ ft. and choosing arbitrarily $t = 0.1$ sec.; we obtain:

$$\frac{\pi^2 \alpha t}{\delta^2} = 234 \gg 1 \qquad \text{III-12}$$

which easily satisfies the inequality.

Because the local heat input in the present experiment is unsteady, it can also be shown that the Biot number, $h\delta/k$ must be very small to insure that the skin temperature does not depart significantly from its initial value before $\partial T/\partial t$ becomes constant in

the direction normal to the skin surface. George and Reinecke[26] require the condition that:

$$h\delta/k \ll \frac{1}{10} \qquad \text{III-13}$$

Choosing a typical value of h for a 30° cone test and inserting values of k and h ($h = 2.0 \times 10^{-3}$ BTU/ft^2-sec°R, $k = 955 \times 10^{-5}$ BTU/ft-sec-°R , $\delta = 0.000833$ ft) one obtains:

$$\frac{h\delta}{k} = 1.74 \times 10^{-4} \ll 0.1 \qquad \text{III-14}$$

Consequently, it is more than sufficient to establish 0.1 sec. as the time after which a uniform $\partial T/\partial t$ will be maintained in the nickel skin.

The upper bound on the time during which data can be recorded is governed by the necessity of limiting diffusion time for heat tangential to the model surface. Manos and Taylor[25] require the condition that the Fourier number based on a characteristic surface length be small enough to minimize diffusion along the surface:

$$\frac{\alpha\tau^2}{\ell^2}\, t \ll 1 \qquad \text{III-15}$$

Choosing $\ell = 1/6$ ft. and $t = \frac{1}{2}$ sec.:

$$\frac{\alpha\tau^2}{\ell^2}\, t = 0.306 < 1 \qquad \text{III-16}$$

The fact that this inequality is not sufficiently satisfied for so short an upper bound on testing time indicates that conduction errors will be present. However, as it will be shown in the section on error analysis, the errors arising from conduction are not of significant

magnitude in the Type II models. The conduction problem in the Type I models cannot easily be calculated due to the discontinuities in wall thickness, material, and metal properties resulting from the stainless steel tips.

Several conclusions should be drawn from the above discussion. Moreover it is obvious that a well-defined lower bound can be imposed on the testing time and that the upper bound is limited by conduction errors tangential to the surface. George and Reinecke[26] have shown that conduction errors may be expressed:

$$E = \frac{\alpha t}{h} \frac{d^2 h}{dt^2} \qquad \text{III-17}$$

Since h can be adequately approximated by $h \propto 1/\sqrt{x}$ over an extensive Reynolds and Mach number range (see Results and Discussion), the equation reduces to:

$$E = \frac{3}{4} \frac{\alpha t}{x^2} \qquad \text{III-18}$$

where x is the distance from the model tip. Qualitatively, one can expect a linear increase of conduction error with time, with the largest errors occuring in the tip region. In regard to the model design one observes that the thin nickel wall satisfies the major design requirements. It should be noted that a metal with lower thermal diffusivity would satisfy the requirement for temperature uniformity normal to the surface and significantly reduce conduction. However, materials in this category such as stainless steel are not so easily machined, their thermodynamic properties are difficult to determine accurately, and there can be inhomogenities in the metal. All things considered, the electroformed nickel shell seems to constitute the most suitable design and material.

F. Heat Transfer Apparatus and Data Reduction

The output of the copper-constantan thermocouples was fed into Philbrick 365 A linear operational amplifiers, which were housed in a temperature oven maintained at a constant 100°F to prevent zero drift. The gain of the amplifiers (either 25 or 50 in the present work) was set high enough to achieve full scale deflection of the 60mv galvanometers in one second or less. An optical arrangement incorporated in a Midwestern oscillograph permitted a visual representation of the galvanometer deflection on photo-sensitive paper. The time lag of the 200 cps amplifier-galvanometer system (order of 50ms) is so brief that it has no bearing on the present experiment. A typical temperature vs. time trace is presented in Figure 7.

Spot calibrations of the thermocouples were performed at room temperature and the boiling point of water. The output voltages were measured with a hand potentiometer and voltages compared to National Bureau of Standards data[27]. Within the three-figure accuracy of the Rubicon hand potentiometer, agreement was excellent, justifying the utilization of the e.m.f. vs. temperature relations of the NBS tables.

At the beginning of each test the model was covered with a water cooled copper shield and maintained at an isothermal wall temperature of approximately 32°F. The flow was suddenly established around the model in 0.03 sec. by the retraction of a pneumatically operated shield. Depending on the heating rate, from 0.5 to 1.5 sec. of data was taken for record purposes. The model was then quickly cooled to 32°F by admitting cold nitrogen gas into the conical shell. Each shell was vented directly into the tunnel where the very low ambient pressures effected a rapid evacuation of the gas when the coolant valve was closed. This procedure was repeated from 16 to 35 times during each run to provide a large statistical sampling

for each thermocouple. Every data point for an individual tunnel run was calculated from an average of four separate thermocouple readings differentiated at five points. Two tests at each stagnation setting were performed as a further indication of the repeatability. Differentiation of the data was accomplished without laborious hand calculations by means of a Model J OSCAR, the output of which was digitized by an IBM keypunch.

G. Error Analysis

Heat transfer data are subject to numerous and large sources of random and systematic error. Throughout the present study careful attention has been paid to possible sources or error which were prevented, minimized or corrected wherever possible. Unfortunately many errors arise from sources beyond the control of the investigator. The major problems encountered and the corrective steps taken are enumerated below.

Systematic Errors

1. Conduction

For a thin-walled heat transfer model, lateral conduction will arise not only from uneven aerodynamic heating but also from initial non-uniformity in the skin temperature. The primary effect is a reduction in measured heating rates at points of maximum heating. Equation III-18 demonstrates that conduction effects increase with elapsed time and decrease with distance from the leading edge.

The mathematical form of the conduction term can be demonstrated directly from the simple heat balance for a differential element of model skin.

$$\rho c_w \delta \frac{\partial T_w}{\partial t} = h (T_{aw} - T_w) + \nabla(k\delta\nabla T) \qquad \text{III-19}$$

Unfortunately, direct evaluation of the conduction term requires $\nabla^2 T$ which cannot be calculated satisfactorily without closely spaced thermocouples surrounding each point where a correction is to be made. Furthermore, random errors in data reduction render determination of the second derivative most inaccurate.

A simpler method for estimating conduction effects has been provided by Conti[28] whose method avoids the necessity for calculating the Laplacian of temperature by assuming an aerodynamic heating distribution of the form $x^{-\frac{1}{2}}$. His analysis is restricted to one-dimensional heat conduction, an initially isothermal surface, constant adiabatic wall temperature, and negligible radiative heat transfer. Since each of these conditions was fulfilled in the present experiment, Conti's method was utilized for an estimation of the conduction effects.

Repeated applications of Conti's approximate solution to typical data revealed that most conduction errors amounted to slightly less than 1%. For example, it was found that 0.3 sec. after retraction of the boots, the conduction error had reached about 0.8% at 0.6" from the model (15°) tip. In only the most limiting cases was conduction a significant cause of error by an elapsed time of $t = 0.3$ sec. The forward station of the 30° cone, located 0.1" from the cone vertex, was the single most limiting case. Here the conduction error reached 12.5% at $t = 0.3$ sec. In such severe instances the error was reduced to about 5% by measuring the slope of the temperature vs. time trace during the initial 0.15 sec. Cases of severe conduction could be recognized easily by the deviation of the trace from a straight line. No actual calculated corrections were deemed necessary since the temperature vs. time data was differentiated as close to the instant of model exposure as the instrumentation response time allowed. Due to this procedure transverse conduction losses were usually less than 1% but never more than about 5%.

An alternate method of treating conduction effects has been proposed by Thomas and Fitzsimmons[29] whose method does not require an assumption of the mathematical form of the heat flux distribution. The correction, which acoounts for non-isothermalities as well as uneven aerodynamic heating, requires a least squares curve fitting to the time history of measured heat transfer coefficients. Although this so-called "T-F Method" is more general, the Conti approach was preferred for the present experiment since the heat flux distribution is known to closely approximate a half power law as required by Conti's analysis.

2. Heat sink effect of thermocouple wires

Due to the fact that the model skin thickness (0.010") and the thermocouple wire diameter (0.005") were of comparable dimensions, it was conceivable that the heat conduction along the wire might cause considerable error to be introduced into the measurement of dT_w/dt . However, an estimation of this error according to the method of McMahon[30] showed the magnitude of the temperature vs. time slope to be underestimated by 2.2% for a typical heat flux and $t = 1$ sec. Although the error introduced is shown to be proportional to the thermocouple wire diameter squared, the use of smaller wire would have seriously complicated model construction.

3. Model skin thickness

Model skin thickness was carefully controlled in manufacture and locally examined to insure that it measured 0.010". The best estimate of average error in machining would be ± .0005" in the temperature vs. time history and therefore ± 5% error in measured heat transfer coefficients.

4. Inaccuracy in the knowledge of the thermodynamic properties of the electroplated nickel

According to Nagel et.al.[29], the specific heat of nickel has been measured to ± 3% for electroformed nickel including variations due to slight differences in purity. The specific heat is also a function of temperature, but for a change in T_w of 10°R, c_p increases only 0.6%[29] at about 460°R.

5. Tunnel axial and transverse gradients

The reference probe measuring P_t was positioned at the station of the model tip so that no correction was needed for axial Mach number gradient. However, corrections were made for the transverse tunnel gradient due to the fact that the pitot probe was $\frac{1}{2}$" off centerline.

6. Source flow effect

Due to the overwhelming theoretical and practical problems involved in the design of a contoured nozzle for a hypersonic, high stagnation temperature wind tunnel, the Princeton nitrogen facilities are equipped with conical nozzles. As a result, the expansion process continues into the test section even though partial contouring is provided by the tunnel boundary layer. A conical rather than uniform free stream results with a shock that is displaced outwards, lower surface pressures, and reduced heat transfer and skin friction coefficients[12]. Although no data is available for the cone, an estimate of the magnitude in the reduction in heat transfer for a conical flow has been shown to be 20% for a wedge at 5 inches from the tip. For a conical geometry where the shock is closer to the body the effect is most likely of at least the same order. Fortunately the tunnel boundary layer provides considerable contouring of the nozzles used in the present investigation. The flows which develop more closely resemble

uniform free streams rather than source flows, and axial Mach number gradients have been shown to be only 0.3 per inch[22]. Although the quantitative effect of this gradient cannot be estimated or corrected for, the measurements reported herein are consistent for the tunnel conditions.

Random Errors

1. Tunnel effects

The major uncertainty in test conditions results from the inference of stagnation temperature from the mass flow rate (See Sec. IIIB). Due to scatter in the flow meter calibrations and to slight variations in the effective orifice area, the accuracy in T_o was limited to $\pm$ 100°K or $\pm$ 5%. The impact of an error in T_o is compounded by the manner in which heat transfer data must be correlated. In the first place, T_o effects the determination of Stanton number as follows:

$$C_H = \frac{\dot{q}}{\rho_\infty U_\infty c_p (T_o - T_{aw})} \sim \frac{\dot{q}}{\rho_\infty U_\infty (T_o - T_w)} \sim \frac{\dot{q}}{\rho_\infty T_o^{3/2}} \sim \frac{\dot{q}}{P_t \sqrt{T_o}} \qquad \text{III-20}$$

Although this effect is relatively small (~2.25%), a more serious inaccuracy arises in knowledge of $Re_{x,\infty}$, the most significant parameter in data correlation. Assuming a linear temperature viscosity relationship for the low free stream temperatures encountered, $Re_{x,\infty}$ varies with T_o as follows:

$$Re_{x,\infty} = \frac{\rho_\infty U_\infty x}{\mu_\infty} \sim \frac{P_\infty \sqrt{c_p (T_o - T_\infty)}}{T_\infty \quad T_\infty} \sim \frac{P_o \sqrt{T_o}\, x}{T_o^{\,2}} \sim \frac{P_o\, x}{T_o^{\,3/2}} \qquad \text{III-21}$$

Considering complete certainty in knowledge of stagnation pressure, the accuracy of a free stream Reynolds number calculation is $\pm$ 11%, by far the largest random or systematic error encountered.

2. Human error in data differentiation

The effect of any error in data differentiation is judged to be negligible due to the large statistical sampling. Each point represents the average of from 12 to 16 independent differentiations of data obtained in a time frame short enough to preclude the possibility of significant variations in tunnel conditions.

Summary

Since errors considered are independent and therefore possibly cumulative , the accuracy in the measurement of Stanton number is estimated to be ± 15% in the proximity of the tip, and ± 11% for the downstream stations. The accuracy of the correlation parameter, $Re_{x,\infty}$, is estimated to be ± 11%.

IV

RESULTS AND DISCUSSIONS

In this section, the sharp cone experimental data is compared with predictions of the classical Blausius-Mangler solution, of the viscous-invisicd analysis[1] of Probstein including transverse curvature[2], of Solomon-Loeb's induced pressure and transverse curvature analysis[21], and of Cheng's viscous layer analysis[3]. The blunt cone results are compared with the local similarity analysis of Lees, and the thin-shock-layer theory of Cheng.

A. Results of the Pointed Cone Experiments

The classical boundary layer predictions for heat transfer is given by Eq. II-8 (note that $\sqrt{c_*}$ is used to account for average temperature in the boundary layer). The expression relates the local inviscid Stanton number to the inviscid cone Reynolds number where

$$St_c \equiv \frac{\dot{q}_w}{\rho_c u_c (H_r - H_w)} \qquad \text{IV-1}$$

By definition the recovery enthalpy H_r is used in the normalization instead of the free stream enthalpy $H_{o,\infty}$. Since radiation losses render the correct measurement of recovery factor almost impossible in hot nitrogen facilities, it is assumed that $r = \sqrt{Pr}$ and that $H_r = \sqrt{Pr}\, H_o$. Inviscid cone values were obtained as described in Section II-A. Under these assumptions the experimental results are compared to the Blausius-Mangler theory for 3°, 5°, 15°, 20° and 30° half-angle cones in Figures 8, 9, 10, 11, and 12, respectively. (Representative data of the entire Reynolds and Mach number range is shown in each figure.) Results for the 3°, 5°, and 15° cones generally fall slightly above the Blausius-Mangler solution. The 20° cone results are scattered about the predicted value, while the 30° cone results

are considerably higher.

In these same figures the heat transfer results are compared to the first order corrections to the boundary layer theory due to the combined effects of induced pressure and transverse curvature. The results of the Probstein[1,2] method according to Eq. II-13 are shown for each cone. The application of Probstein's analysis to the slender 3° and 5° cones results in a large overestimation of the heat transfer, but the agreement is fairly good for the 15° and 20° cones where the data generally falls between Probstein's analysis and the boundary layer result. Predicted increases to the Mangler value for the 30° cone are small, and the 30° results lie considerably above the first order corrected solution also. The fact that the heat transfer to the 3° and 5° cones is so highly overestimated may be attributed to the fact that the transverse curvature parameter $(\Delta/r_o(x))_M$ (Eq. II-11) is so large in each of these cases. The theoretical analysis requires that $(\Delta/r_o(x))_M$ be less than unity, because the solution involves series expansions of a small parameter proportional to $(\Delta/r_o(x))_M$. For the 3° cone a typical value of $(\Delta/r_o(x))_M$ is 8.9 while for the 5° cone it may be 3.05. Therefore, the expansion is invalid, and the results of the analysis are inapplicable to the 3° and 5° results of the present experiment. The zero-order Blausius-Mangler theory gives a much more accurate estimate than may be obtained by applying first order corrections as proposed by the Probstein analysis. However, the agreement is most likely fortuitous and may be attributed to the fact that the data for the slender cones tends to fall below the combined boundary layer results plus first order corrections. At the lower rarefactions ($W \leq 3$) of the present study, slender cone data might be expected to begin to tend toward the free molecular value. Evidence of this phenomenon will be discussed in greater detail below.

The heat transfer data are correlated in terms of the parameters proposed by Cheng[3] and modified by Waldron[8] for the viscous layer regime in Figs. 13, 14, 15, 16 and 17:

$$\frac{C_{H,\infty}}{\sin\theta_c}(1 - T_w/T_o) \quad \text{vs.} \quad W = \frac{Re_{x,\infty}}{M_\infty^2}\frac{1}{\gamma c_* \cos\theta_c} \qquad \text{IV-2}$$

Cheng originally suggested that $C_{H,\infty}/\sin\theta_s$ be used in the correlation, but for simplicity θ_s has been replaced by θ_c. To account for the variation in wall and stagnation conditions the ordinates have been modified by the factor $(1 - T_w/T_o)$ as suggested by Waldron[8]. The constant used in the linear viscosity-temperature relationship is defined such that:

$$T_* = T_o\,[1 + 3(T_w/T_o)]/6 \qquad \text{IV-3}$$

as proposed by Cheng[5]. In his later viscous layer analysis[3] he suggested that the reference temperature for conical flows be taken as:

$$T_* = T_w/2 + T_o\left(\frac{1}{2} - \frac{1}{3}\cos^2\theta_c\right) \qquad \text{IV-4}$$

As θ_c decreases the latter reference temperature reduces to the former, which can be shown to be the average temperature across a locally similar, hypersonic boundary layer on a flat plate. No significant difference arises in the two reference temperatures until $\theta_c \cong 20°$. For the 20° and 30° cone of the present study c_* would be reduced by 5% and 10% respectively had Eq. IV-4 been used. For the 20° and 30° cone the data is more effectively correlated using Eq. IV-3, hence this equation is used throughout.

Even though Cheng's heat transfer parameters were proposed for the viscous-layer regime for $W \leq 10$, they have proven valid for

correlating heat transfer data over a wide range of heating rates, cone angles, and Reynolds numbers. However, in the present results a slight dependence of $C_{H,\infty}/\sin\theta_c$ can be observed. For a given value of W a general increase in $C_{H,\infty}/\sin\theta_c$ occurs as cone angle decreases. This increase may be observed consistently except in the case of the low Reynolds number, 30° results which fall higher than the corresponding 20° results. A viscosity relationship based on T'_* as defined by Eq. IV-4 would not affect this trend for the smaller cone angles where the neglected transverse curvature effects are much more significant.

A modification of the boundary layer theory to include the first order effects of induced pressure and transverse curvature has been proposed by Solomon-Loeb[21]. Results of their Pohlhaussen solution are presented with the data for each cone in Figure 13-17. It is important to note that the Solomon-Loeb solution is not limited to small values of the transverse curvature parameter $(\Delta/r_o(x))_M$ as was Probstein's analysis. In fact the former authors give a limiting solution for infinite transverse curvature effects (Eq. II-16) which is of course valid for very slender cones at hypersonic Mach numbers. In direct contrast the validity of Probstein's results for slender cones would be limited to supersonic Mach numbers for the present, low Reynolds number range.

Agreement of the heat transfer results and the Pohlhaussen solution are excellent for the 15°, 20°, and 30° cases throughout the Reynolds number range. For the slender 3° and 5° cones the results are good for $W \geq 100$. The range of W covered in the present study is particularly interesting because the first evidence of the departure of the results from the boundary layer theory may be observed. The 3° and 5° results appear to depart from the Solomon-Loeb solution at $W \simeq 60\text{-}90$ and tend toward the viscous layer

analysis of Cheng[3]. These results are consistent with the observation of Waldron[8] who commented on a similar departure of the results of Wilkingson and Harrington[7] in the neighborhood of $W = 100$. As the boundary layer limit for his observation, Waldron employed Probstein's first order transverse curvature correction (Eq. II-12). This procedure is incorrect for two reasons: In the first place Probstein's analysis is invalid for $(\Delta/r_o(x))_M \gg 1$, and secondly Waldron failed to consider the induced pressure correction to the Mangler solution (Eq. II-10). The 6.3° results of Reference 7 actually agree well with the present 5° results as well as to the proper boundary layer limit. Departure from the Solomon-Loeb solution of the shock tunnel data occurs at $W = 90$.

For the larger half-angled cones departure from the boundary layer result does not occur until the flow is more rarefied at lower values of W. The 15° cone results follow the Solomon-Loeb solution at least as far as $W = 15$, while evidence of departure for the 20° and 30° cones can be first observed at $W \simeq 3$.

Selection of a particular limiting case for the Pohlhaussen solution was made with several considerations in mind. The transverse curvature parameter $\overline{\chi}$ can be related to W by a constant for a given cone angle. This constant is large enough so that $\overline{\chi}$ is not sufficiently small to apply the limiting solution for $\overline{\chi} \to 0$ except for the 3° cone. For cones of larger half angles $\overline{\chi}$ remained close enough to unity to cause Eq. II-16 to blow up because of the denominator $\overline{\chi} \log \frac{1}{\overline{\chi}}$. Therefore, the limiting solution for small transverse curvature, Eq. II-17, was utilized for comparison to the 5°, 15°, 20°, and 30° cones.

B. Results of Blunt-Nose Cone Experiments

In an effort to determine the validity of several theoretical

treatments of the blunted cone, experimental results were obtained on spherically-capped right circular cones. A wide range of length-to-nose radii is investigated for each of the 5°, 15°, 20°, and 30° cones.

The experimental results were compared to the theoretical calculation of Lees[4] whose result for the heat transfer distribution on the conical surface of a blunt cone may be written:

$$\frac{\dot{q}_w}{(\dot{q}_w)_o} = A(\theta_c) \frac{x/r_o}{[B(\theta_c) + (x/r_o)^3]^{1/2}} \qquad \text{IV-5}$$

for

$$\frac{x}{r_o} \geq \cot\theta_c \qquad \text{IV-6}$$

x, the distance along the surface measured from the virtual tip is related to the actual distance from the stagnation point by

$$x = S + r_o [\cot\theta_c - (\pi/2 - \theta_c)]$$

The function $A(\theta_c)$ and $B(\theta_c)$ depend on γ, M_∞, and θ_c (Ref. 4). The local heat flux must be normalized by the stagnation point heat transfer which was not measured in the present experiment. Consequently, $(q_w)_o$ was calculated from the Lees expression:

$$(q_w)_o = \frac{\sqrt{\frac{2}{2}} P_r^{-2/3} \sqrt{(\rho_e \mu_e)_o} \sqrt{u_\infty} \; h_{se} \; G(M_\infty, \bar{\gamma}, \gamma_\infty)}{\sqrt{r_o}} \qquad \text{IV-7}$$

Results for the 5°, 15°, 20° and 30° cones are presented in Figures 18-21. The several test section conditions represented cover the entire Mach and Reynolds ranges. The 5° results show neither qualitative nor quantitative agreement with the simplified Lees

expression. Data points spanning the entire Reynolds number range fall within ± 8% , it is clear that the Lees formulation does not apply to very small half-angle cones of the present bluntness. Ratios of $q_w/(q_w)_o$ for the 15° , 20° and 30° cones correlate well over the range of conditions, and at least qualitative agreement with the theory is exhibited by the slopes of the data. However, values of $q_w/(q_w)_o$ fall significantly above the theoretical distribution. For the 15° cone this discrepancy ranges from 25% near the leading edge to 45% near the trailing edge, $22\frac{1}{2}$ nose radii downstream. The predicted heat transfer is underestimated by approximately 35% to 55% for the 20° cone, and by about 24% to 35% for the 30° cone. Due to the consistent underestimation of the ratio $q_w/(q_w)_o$, one must examine the possibility of an underestimation of the stagnation point heat transfer. By comparison of the Lees result to the experimentally verified solution of Fay and Riddell[31], one finds agreement accurate to less than 3%. It is therefore unlikely that the calculated values of $(q_w)_o$ were seriously in error.

The experimental blunt cone results were compared to the zero order predictions of Cheng[5] who proposed the correlation parameter

$$\frac{M_\infty^2(\epsilon k)^{1/4} C_{H,\infty}}{\theta_c^2 \bar{X}_t} \quad \text{vs.} \quad \frac{\theta_c^2 S}{\sqrt{\epsilon k}\, t}$$

The domain of validity of Cheng's formulation is characterized by several restrictions which govern the degree of accuracy of the analysis in the inviscid-flow region as well as the boundary layer. These conditions, which were discussed above, may be summarized and examined as follows:

Theoretical Assumption	Experimental Condition
1) $\gamma \rightarrow 1$	$\gamma \rightarrow 1.4$
2) $\epsilon \equiv {}^{\gamma-1}/_{\gamma+1} \ll 1$	$\epsilon = 1/6$
3) $(1/2)\theta_c^{\,2(\gamma-1)/\gamma} \ll 1$	$.124 < (1/2)\theta_c^{\,2(\gamma-1)/\gamma} < .345$
4) $M_\infty^{\,2}\,\theta_c^{\,2} \gg 1$	$M_\infty^{\,2}\,\theta_c^{\,2} = 2.2$ for 5°
	19.8 for 15°
	35.2 for 20°
	79.2 for 30°

The several restrictions listed are mutually exclusive in that they require a large flow deflection angle to satisfy (4) and at the same time a small deflection angle to satisfy (3). The latter two conditions are more nearly satisfied by the 15° cone. The limit of validity of the strong shock condition ($M_\infty^{\,2}\,\theta_c^{\,2} \gg 1$) is approached by the 5 cone while the limit of Cheng's small perturbation velocity requirement ($1/2\,\theta_c^{\,2(\gamma-1/\gamma)} \ll 1$) is approached with the 30° cone.

Results of the comparison of the data to Cheng's zero-order shock layer theory are shown in Figures 22-25. The nose drag coefficient, k , used in the correlation was calculated according to a modified Newtonian pressure distribution for a spherically blunted nose (See e.g. Ref. 32). The numerical agreement of the data with the theory is generally poor, and the power law slope predicted is incorrect. However, the correlation parameters themselves seem to be quite good since the data for the full range on cone angles and Reynolds numbers follow the same power law curve (See Fig. 26). The poor agreement of theory and experiment is most likely due to a breakdown of the assumptions of the analysis and the zero-order nature of the solution. Where the small perturbation velocity assumption breaks down for the larger cones, the heat transfer is underestimated; and

where the shock weakens for cones of small half-angles, the heat transfer is underestimated.

The predicted oscillatory decay is evidently associated with the zero-order nature of the solution and does not have the physical significance of a skipping and reattaching shock layer as Cheng suggested. No oscillations in the data are observed in the results for any cone angle.

C. Comparison of Sharp and Blunt Cone Results

Due to the high heat transfer rates encountered in the stagnation regions of actual flying vehicles, at least some nose-blunting is required to reduce the heating problem to manageable proportions. For practical engineering applications it is of interest to know the convective heat transfer rates at equal distances from the virtual tip of a sharp or blunt cone of a given half-angle. In Figures 27 ond 28 the ratios of the blunt cone heat transfer parameters, $C_{H,b}$, to the sharp cone heat transfer parameters, $C_{H,s}$, are presented for the full Reynolds number range for the 5° and 15° cones. Since these cones were of the interchangeable tip variety, it was possible to change tips without affecting the alignment of these models. Ratios of these parameters are not presented for the Type II, 20° and 30° cones for several reasons: 1) Installation of separate sharp and blunt models made it impossible to ensure exactly the same alignment or skin thicknesses, and 2) Due to calibration problems the 30° cones were tested at Reynolds numbers which differed by more than 10% between the sharp and blunt cases. These uncertainties and the differences in test conditions completely obscure effects due to bluntness alone. However, Lees[4] has shown that variations between heating rates of sharp and blunt cones of large half-angles are small.

For the 5° cone the reduction in heat transfer due to bluntness

is as large as 20%. For $x = 2"$ the blunt cone heating rates on the 5° cone are considerably larger than the sharp cone rates. This result is consistent with the data of Feik[12], who tested 5° cones of the same bluntnesses under similar testing conditions. At locations in the vicinity of $x/d = 13$ the blunt cone heating rates fall about 20% below the sharp cone results. For the lower Reynolds number cases the bluntness effects disappear in the neighborhood of $x/d = 24$, while the blunt-cone entropy layer for the higher Reynolds number case still has considerable influence beyond that point.

For the 15° cone the influence of bluntness is greatest at the first data point, $x/d = 4$. Here the blunt cone results fall some 20% below the sharp cone heating rates. The influence of the blunted tip gradually decreases as one moves further downstream on the cone. At x/d values of about 10, no further bluntness effects are detected in either of the higher or lower Reynolds number cases.

V

CONCLUSIONS

The most important results of the present study are:

(1) The classical boundary-layer solution provides a good estimate of local heat transfer distributions for the Reynolds and Mach number ranges investigated when an appropriate reference temperature (T_*) is chosen for the linear temperature-viscosity relationship.

(2) The large rise in heat transfer predicted by Probstein[1,2] in his transverse curvature and boundary-layer displacement analyses is not observed experimentally even for the 3° cone. However, Cheng's[3] viscous-layer solution for $W < 10$ is quite accurate in this portion of the transition regime between continuum and free molecular flow. Although the continuity, momentum and energy equations solved by Probstein and Cheng are basically the same, a substantial difference is evident in the numerical results due to the fact that Probstein's outer boundary conditions are given by the external inviscid flow whereas Cheng's outer boundary conditions are given at the shock. Since the present results support Cheng's predictions, the conclusion that transport at the shock is important in reducing heat transfer below the classical-boundary layer limit at low Reynolds numbers is reinforced.

(3) The limiting solution of Solomon-Loeb[21], which includes transverse curvature, is valid over the entire cone angle range (except 3°, low Reynolds number) for $W < 10$.

(4) Cheng's[3] parameter, W, is valid for correlating heat transfer data over the entire Reynolds number and cone-angle range. The experimental data expressed as $(C_H/\sin\theta_c)(1-T_w/T_o)$ exhibit only a small dependence on cone angle. The increase in heat transfer for small cone angles is attributed to transverse curvature; however, the rise is much smaller than that predicted by Probstein.

(5) For engineering design purposes the theoretical analyses of both Cheng[3] and Solomon-Loeb[21] are completely adequate. For the higher Reynolds numbers, $W < 90$, the classical boundary layer solution is quite satisfactory.

(6) The predictions of Lees'[4] simplified blunt cone method fall below the experimental data for all cone angle tested.

(7) Cheng's[5] bluntness parameter correlates data for the full Reynolds and cone-angle range, although the oscillations predicted by his thin shock layer theory are not observed.

(8) The smaller the cone angle the more effective is nose blunting in reducing heat transfer below the equivalent sharp cone results. The 5° blunt cone results exhibit a 20% reduction in heat transfer as far as twenty nose diameters downstream. The 15° results show a 20% reduction at four diameters while no reduction at all is evident twelve diameters downstream. The 20° and 30° cone data exhibited heat transfer results which were insensitive to nose blunting less than one nose diameter downstream.

The following recommendations are provided for extensions of the present study:

(1) The uncertainty in wind tunnel conditions could be substantially reduced if the graphite heating elements were pre-treated to eliminate carbon flaking and subsequent deposits in the nozzle throat.

(2) Heat transfer is sensitive to stagnation conditions. Although stagnation pressure can be determined precisely with Heise gages, stagnation temperature is difficult to determine accurately. Meticulous care should be taken in the calibration of nitrogen facilities for heat transfer experiments.

(3) Further heat transfer investigations are needed at lower Reynolds numbers than could be obtained in the present facilities

in order that the transition regime between continuum and free-molecular flow can be more fully understood.

REFERENCES

1. Probstein, R. F.: Interacting Hypersonic Laminar Boundary Layer Flow over a Cone. Brown University, Division of Engineering, TR AF-2798/1, March 1955.

2. Probstein, R. F. and Elliott, E.: The Transverse Curvature Effect in Compressible Axially Symmetric Laminar-Boundary-Layer Flow. Journal of Aeronautical Sciences, Vol. 23, No. 3, March 1956.

3. Cheng, H. K.: The Blunt-Body Problem in Hypersonic Flow at Low Reynolds Number. Cornell Aeronautical Laboratory, Rept. AF-1285-A-10, June 1963.

4. Lees, Lester: Laminar Heat Transfer over Blunt-Nosed Bodies at Hypersonic Flight Speeds. Jet Propulsion, Vol. 26, No. 4, pp. 259-269, April 1956.

5. Cheng, H. K.: Hypersonic Flow with Combined Leading-Edge Bluntness and Boundary-Layer Displacement Effect. Cornell Aeronautical Laboratory, Rept. 1285-A-4, August 1960.

6. Feik, R. A., Genchi, A. and Vas, I. E.: A Study of Merging on Cones. Rarefied Gas Dynamics, Vol. I, p. 493, L. Trilling and H. Wachman, ed., Academic Press, New York, 1969.

7. Wilkingson, D. B. and Harrington, S. A.: Hypersonic Force, Pressure, and Heat Transfer Investigations of Sharp and Blunt Slender Cones. Arnold Engineering Development Center, Rept. TDR-63-177, August 1963.

8. Waldron, H. F.: Viscous Hypersonic Flow over Pointed Cones at Low Reynolds Numbers. AIAA Journal, Vol. 5, No. 2, pp. 208-218, 1967.

9. Burke, A. F. and Dowling, E. D.: Aerodynamic Aspects of the Use of a Blunt, Slender Cone as an Air-Data Probe at Hypersonic Speeds. Cornell Aeronautical Laboratory, CAL Rept. No. AA-1577-Y-4, November 1962.

10. Wittliff, Charles E. and Wilson, Merle R.: Heat Transfer to Slender Cones in Hypersonic Air Flow, Including Effects of Yaw and Nose-Bluntness. Journal of the Aerospace Sciences, Vol. 29, No. 7, July 1962.

11. Griffith, B. J. and Lewis, Clark H.: Laminar Heat Transfer to Spherically Blunted Cones at Hypersonic Conditions. AIAA Journal, Vol. 2, No. 3, p. 438-444, March 1964.

12. Feik, R. A.: An Experimental Study, in Low Density Hypersonic Flow over a Cone, of the Effects of Slight Bluntness. MSE Thesis, Princeton University, 1969.

13. Vas, I. E.: An Experimental Study of the Flow about a Slender Cone at Hypersonic Speeds. Ph.D. Thesis, New York University, 1970.

14. Gregorek, G. M.: Viscous Effects of Blunt Cones at Low Reynolds Numbers and Hypersonic Speeds. Aerospace Research Laboratories, ARL 69-0006, January 1969.

15. Taylor, G. I. and Maccoll, J. W.: The Air Pressure over a Cone Moving at High Speeds. Proc. Roy. Soc. (London) A, 139, p. 278-311, 1933.

16. Hayes, W. D. and Probstein, R. F.: Hypersonic Flow Theory. Ch. VIII, p. 284-325, Academic Press, New York, 1959.

17. Young, A. D.: Modern Developments in Fluid Dynamics, High Speed Flow, Vol. 1, Chapter X, Ed. by L. Howarth, Oxford University Press, Oxford, 1953.

18. Eckert, Ernst R. G.: Study on Heat Transfer at High Speeds. WADC TR 54-70, April 1954.

19. Chapman, D. R. and Rubesin, M. W.: Temperature and Velocity Profiles in Compressible Laminar Boundary Layers with Arbitrary Distribution of Surface Temperatures. Journal of the Aeronautical Sciences, Vol. 16, 1949.

20. Schlicting, H.: Boundary Layer Theory. McGraw-Hill, New York, 1955.

21. Soloman, Jay M. and Loeb, Bernard S.: An Approximate Solution for Compressible Axisymmetric Laminar Boundary Layers Including the Effects of Transverse Curvature. NOLTR 67-108, July 1967.

22. Vas, I. E. and Koppenwallner, G.: The Princeton University High Pressure Hypersonic Nitrogen Tunnel N-3. Princeton University, Dept. of Aeronautical Engineering Rept. 690, July 1964.

23. Vas, I. E. and Harvey, J. K.: Further Development of a Graphite Heater for High Pressure Nitrogen Operation. Princeton University, Dept. of Aeronautical Engineering Rept. 667, September 1963.

24. Michels, A., Lunbeck, R. J. and Wolker, G. J.: Thermodynamic Properties of Nitrogen as Functions of Density and Temperature Between -125° and 150° C and Densities up to 760 Amagat. Phisica XVII No. 9, September 1951.

25. Manos, W. P. and Taylor, D. E.: Analysis of Interpretation of Data on Thin-Skinned Heat Transfer Models. Journal of Heat Transfer 84, p. 191-192, 1962.

26. George, A. R. and Reinecke, W. G.: Conduction in Thin-Skinned Heat Transfer and Recovery Temperature Models. AIAA Journal, Vol. 1, No. 8, Tech. Note, p. 1956-1958, 1963.

27. Shenker, Henry; Lauritzen, John I.; Corruccini, Robert J. and Lonberger, S. T.: Reference Tables for Thermocouples. NBS Circular 561, April 1955.

28. Conti, Raul J.: Approximate Temperature Distributions and Streamwise Heat Conduction Effects in the Transient Aerodynamic Heating of Thin-Skinned Bodies. NASA Tech. Note D-895, September 1961.

29. Nagel, A. L., Fitzsimmons, D. H. and Doyle, L. B.: Analysis of Hypersonic Pressure and Heat Transfer Tests on Delta Wings with Laminar and Turbulent Boundary Layers. NASA CR-533, 1966.

30. McMahon, Howard M.: An Experimental Study of the Effect of Mass Injection at the Stagnation Point of a Blunt Body. GALCIT Hypersonic Research Memorandum No. 42, May 1958.

31. Fay, J. A. and Riddell, R. R.: Theory of Stagnation Point Heat Transfer in Dissociated Air. Journal of the Aeronautical Sciences, Vol. 25, No. 2, February 1958.

32. Chernyi, G. G.: Introduction to Hypersonic Flow. Fizmatgiz, Moscow, 1959. English transl. (R. F. Probstein, transl. and ed.), Academic Press, New York, 1961.

TABLE I

Experimental Conditions

Quantity	Unit	N-3, N-5 Tunnel 10° Conical Nozzle			N-3 Tunnel 6° Conical Nozzle	
P_p	psia	2000	3000	5000	2000	4000
T_o	°K	2000	2000	2000	2000	1700
P_2	psia	0.093	0.110	0.150	0.420	0.670
P_∞	psia	1.3×10^{-4}	1.4×10^{-4}	1.7×10^{-4}	1.0×10^{-3}	1.5×10^{-3}
T_∞	°K	18	16	5	32	25
M_∞	-	23.8	25	26.2	17.5	18.5
λ_∞	inches	5.0×10^{-3}	4.0×10^{-3}	2.8×10^{-3}	1.5×10^{-3}	7.0×10^{-4}
$Re_{x,\infty}$	1/in.	7100	9200	14,000	17,600	39,300
$\bar{V}_{x,\infty}$	in.	0.241	0.223	0.190	0.110	0.079
$\bar{X}_{x,\infty}$	in.	138	140	143	34.1	27
W	1/in.	12.3	14.4	19.6	89	175

TABLE II

Half Angle θ_c	Type	R_o	Based inches	Length (inches from virtual apex)
3°	I	.002	.750	7.17
5°	I	.002 .1125	1.50	8.59
10°	I	.002 .105	1.50	4.32
15°	I	.002 .1125	1.50	2.90
20°	II	.002	1.00	1.46
20°	II	.1125	1.00	1.46
30°	II	.002	1.00	1"
30°	II	.1125	1.00	1"

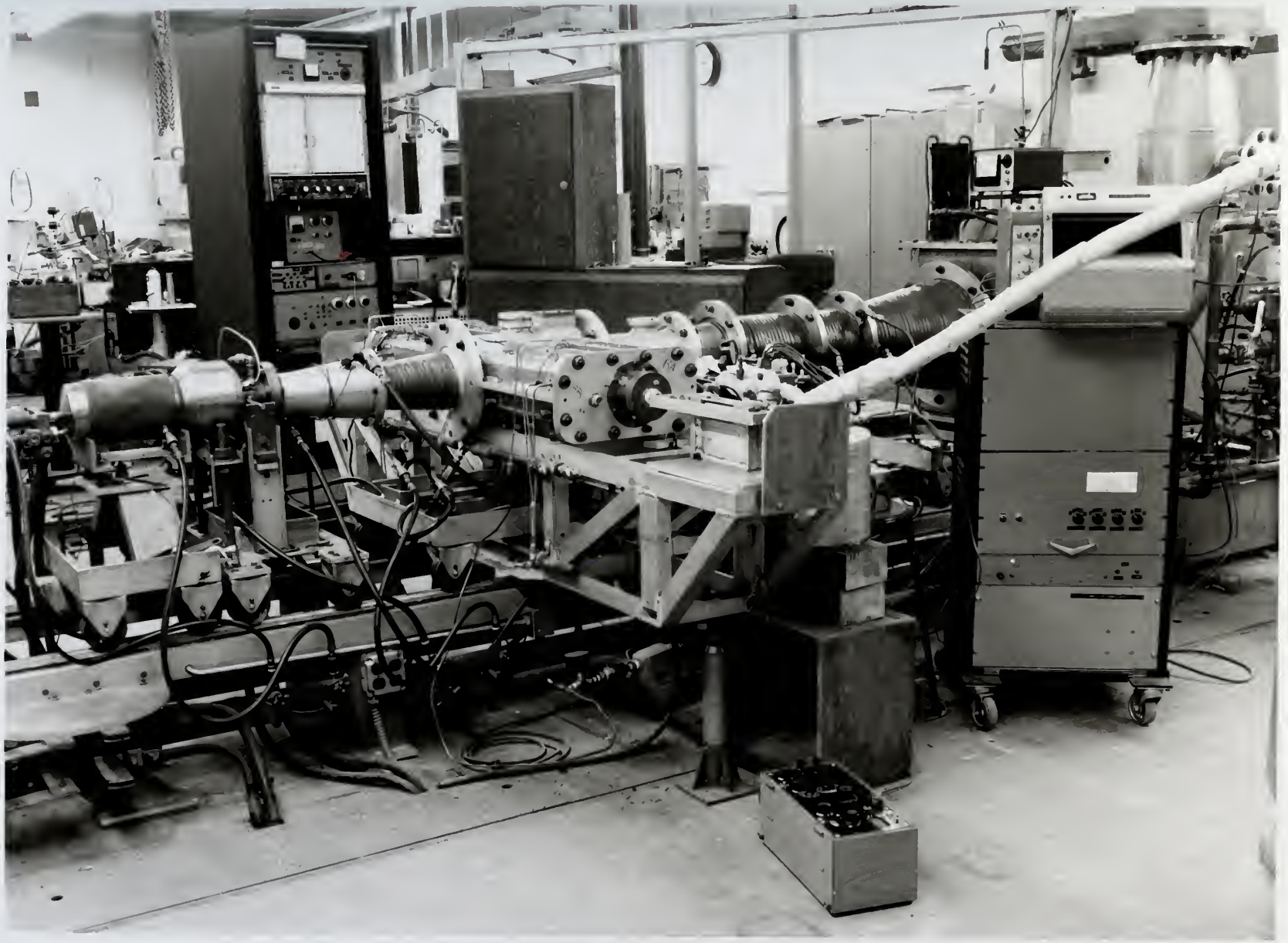

Figure 1 - The Princeton Hypersonic Nitrogen Tunnel N-3

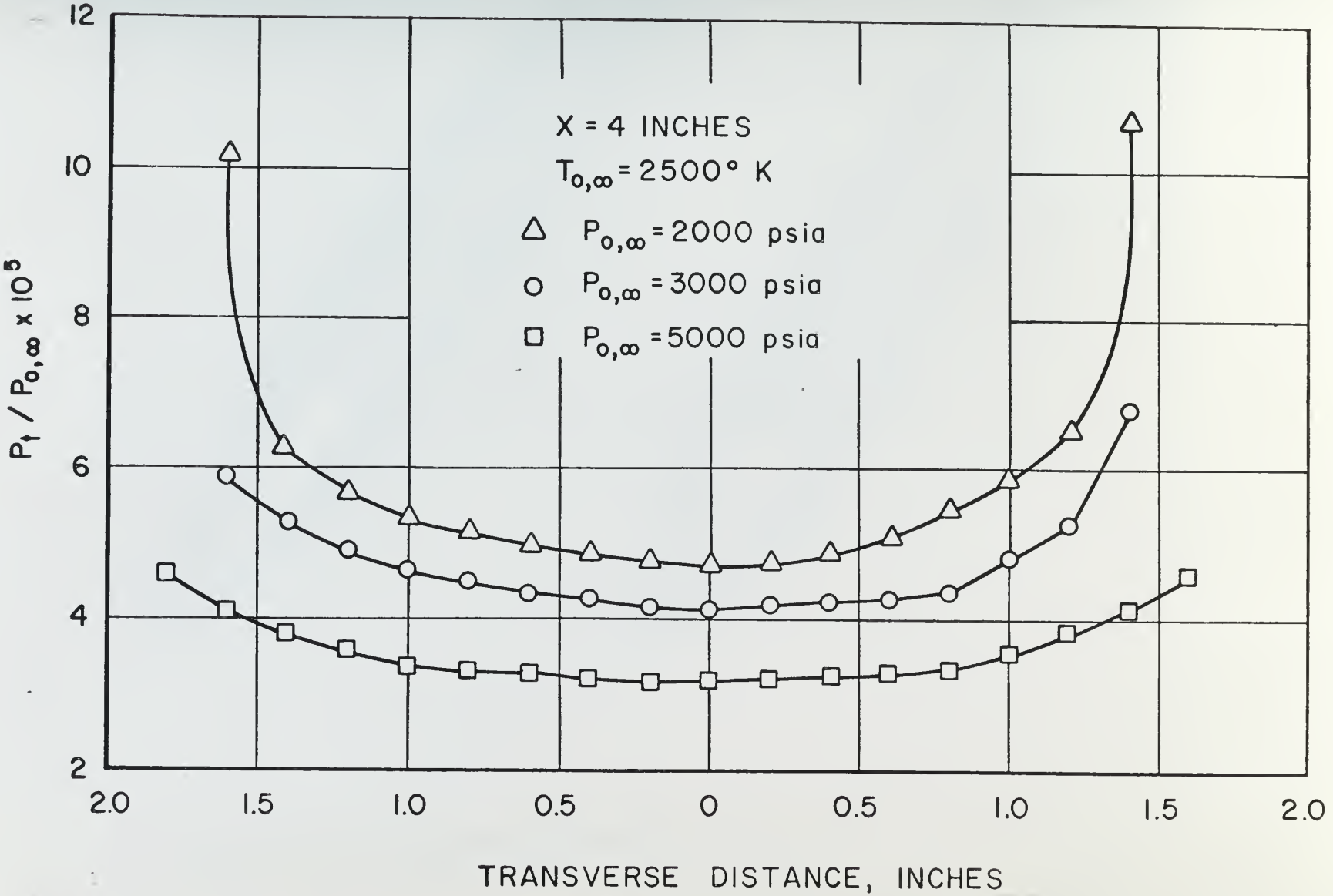

Figure 2 Pitot Pressure Profiles (Nitrogen Tunnel N-3)

Figure 3 - 15° Blunt and 20° Sharp, Type I Heat Transfer Models

Figure 4 - 3° Sharp, Type I Model; 20° Sharp and 20° Blunt, Type II Heat Transfer Models

G-2482

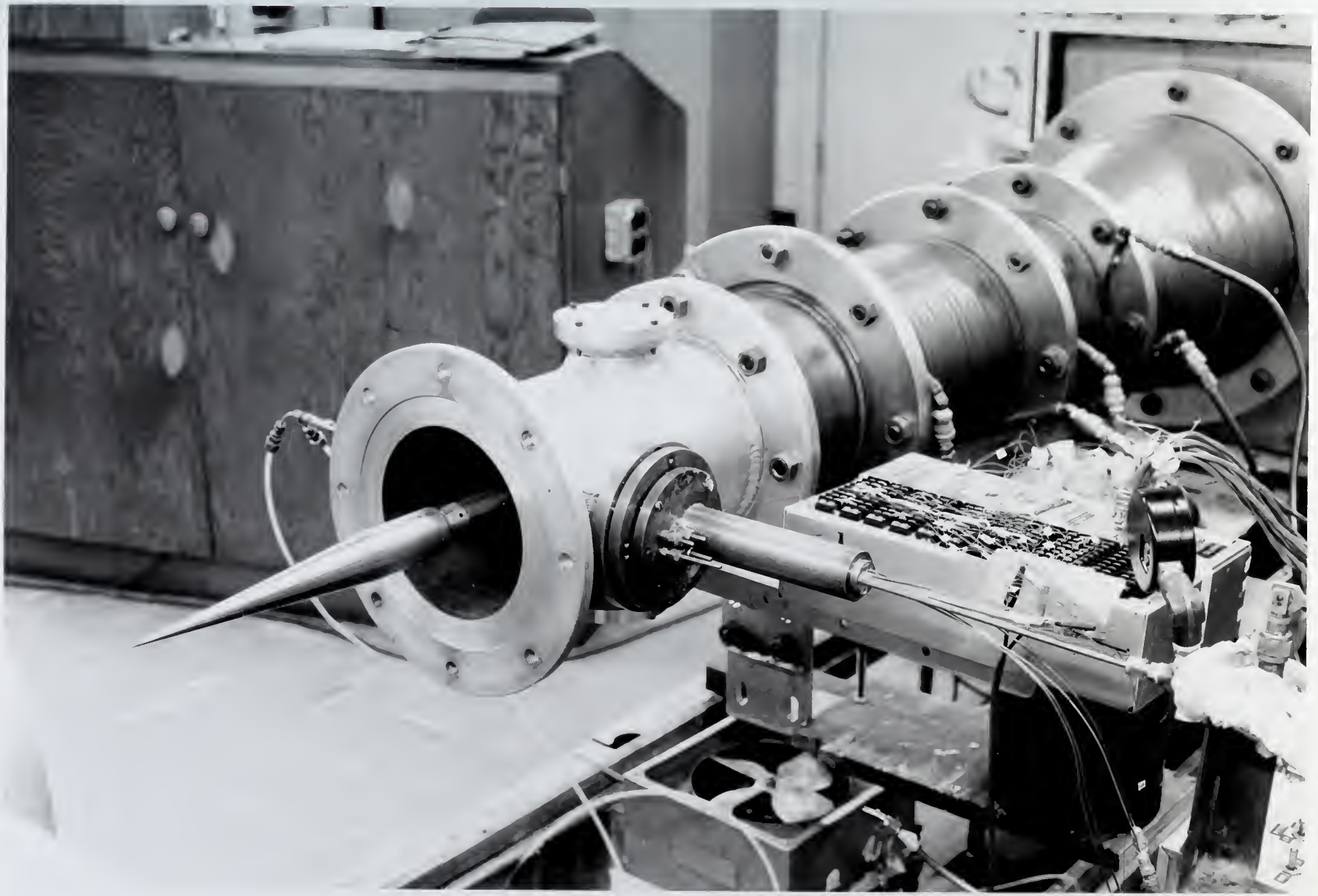

Figure 5 - 5° Heat Transfer Model Mounted in N-3

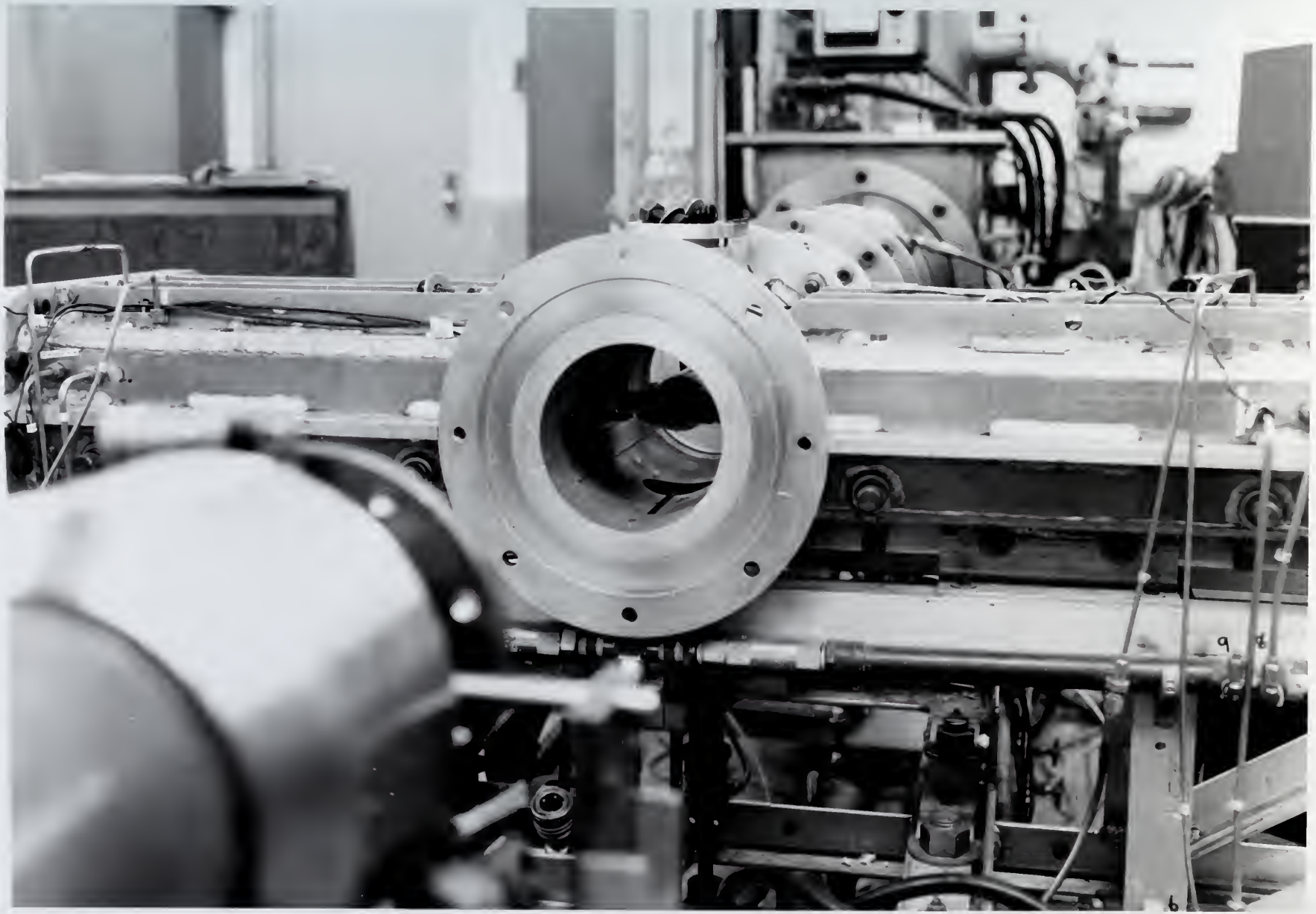

Figure 6 - Pneumatically Operated Boots Shielding Model In Test Section

G-2481

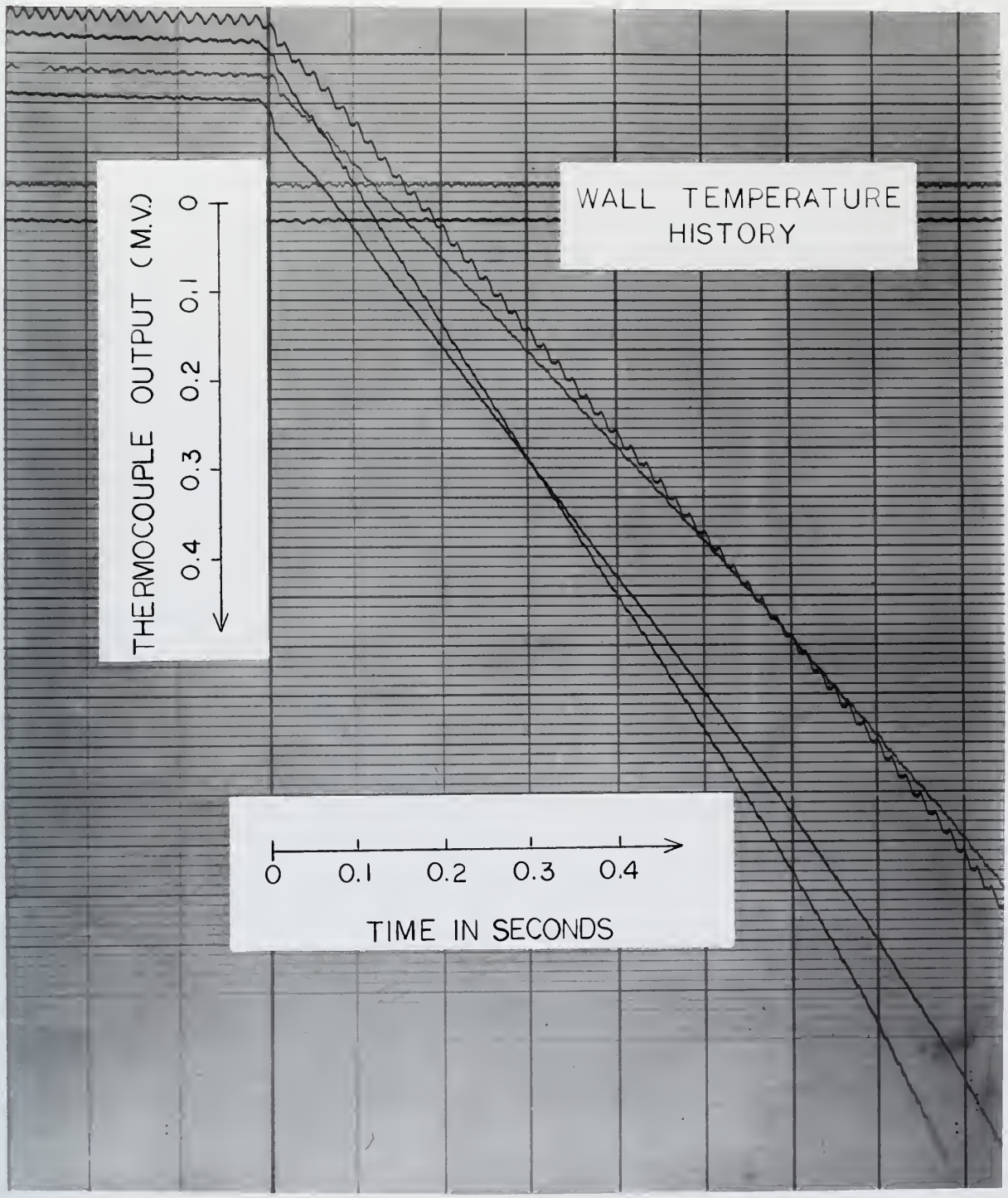

Figure 7. Typical Oscillograph Traces of Voltage vs. Time for the 20° Spherically Blunted Cone.

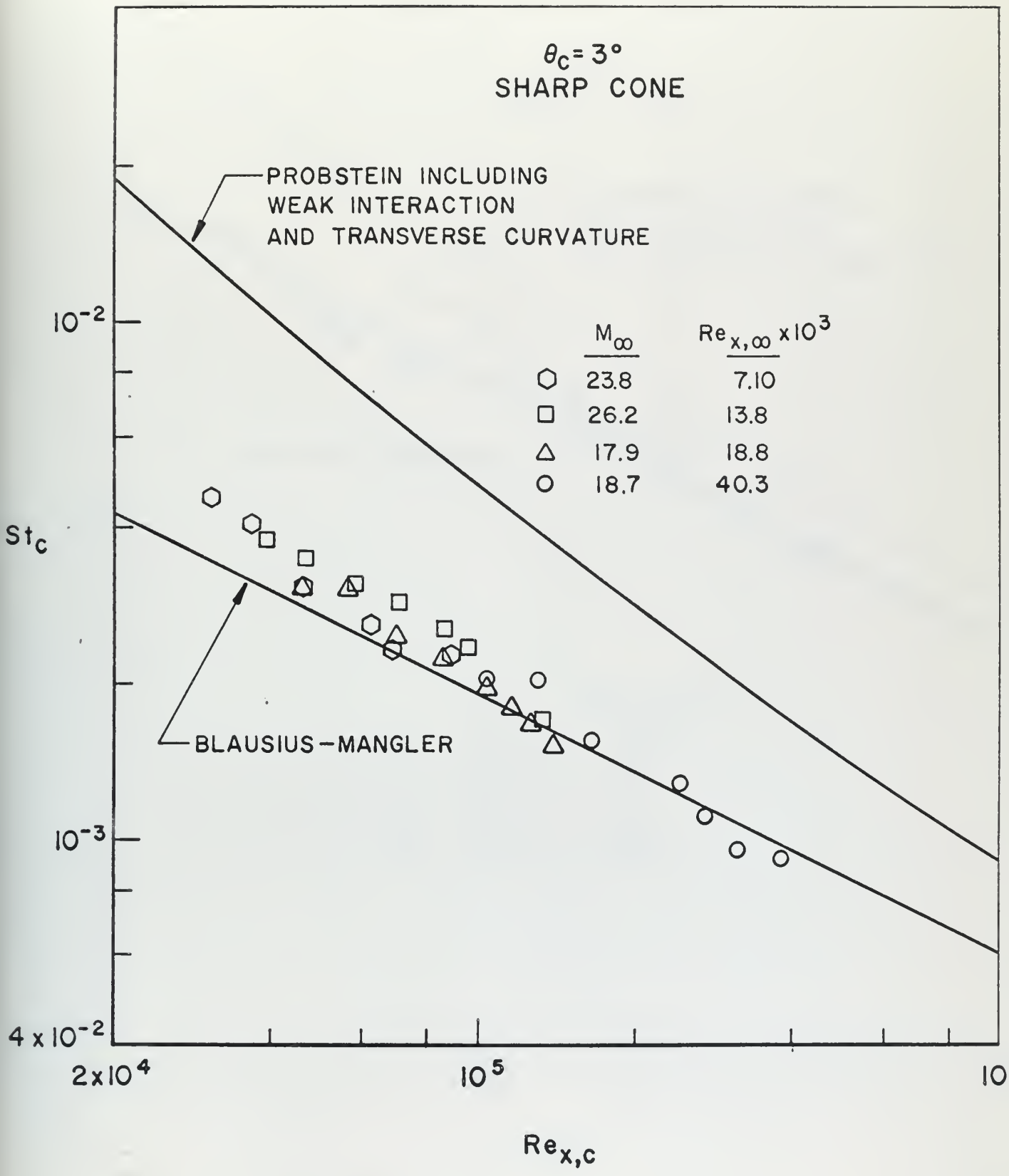

Figure 8 3° Sharp Cone Stanton Number vs. Reynolds Number

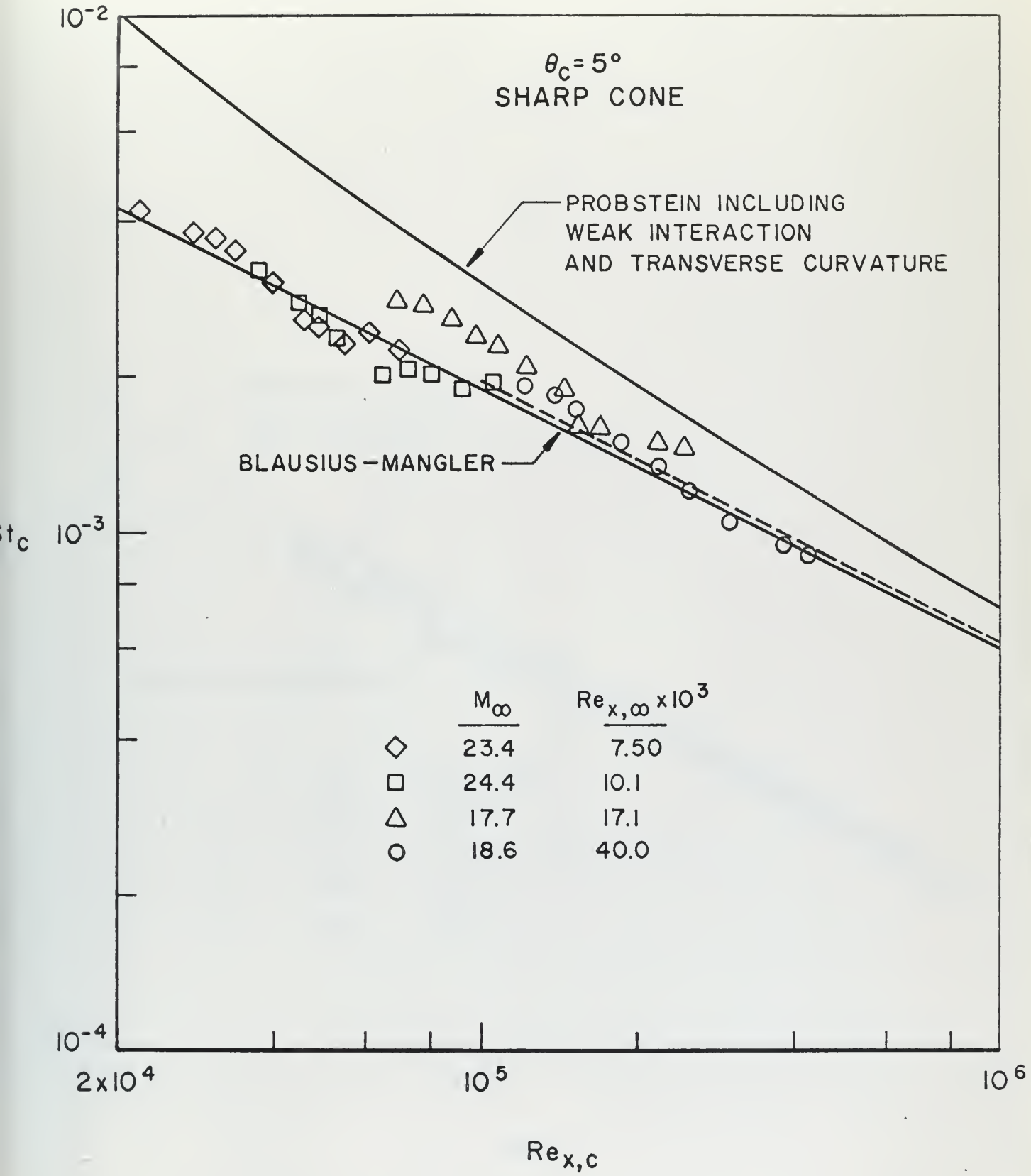

Figure 9 5° Sharp Cone Stanton Number vs. Reynolds Number

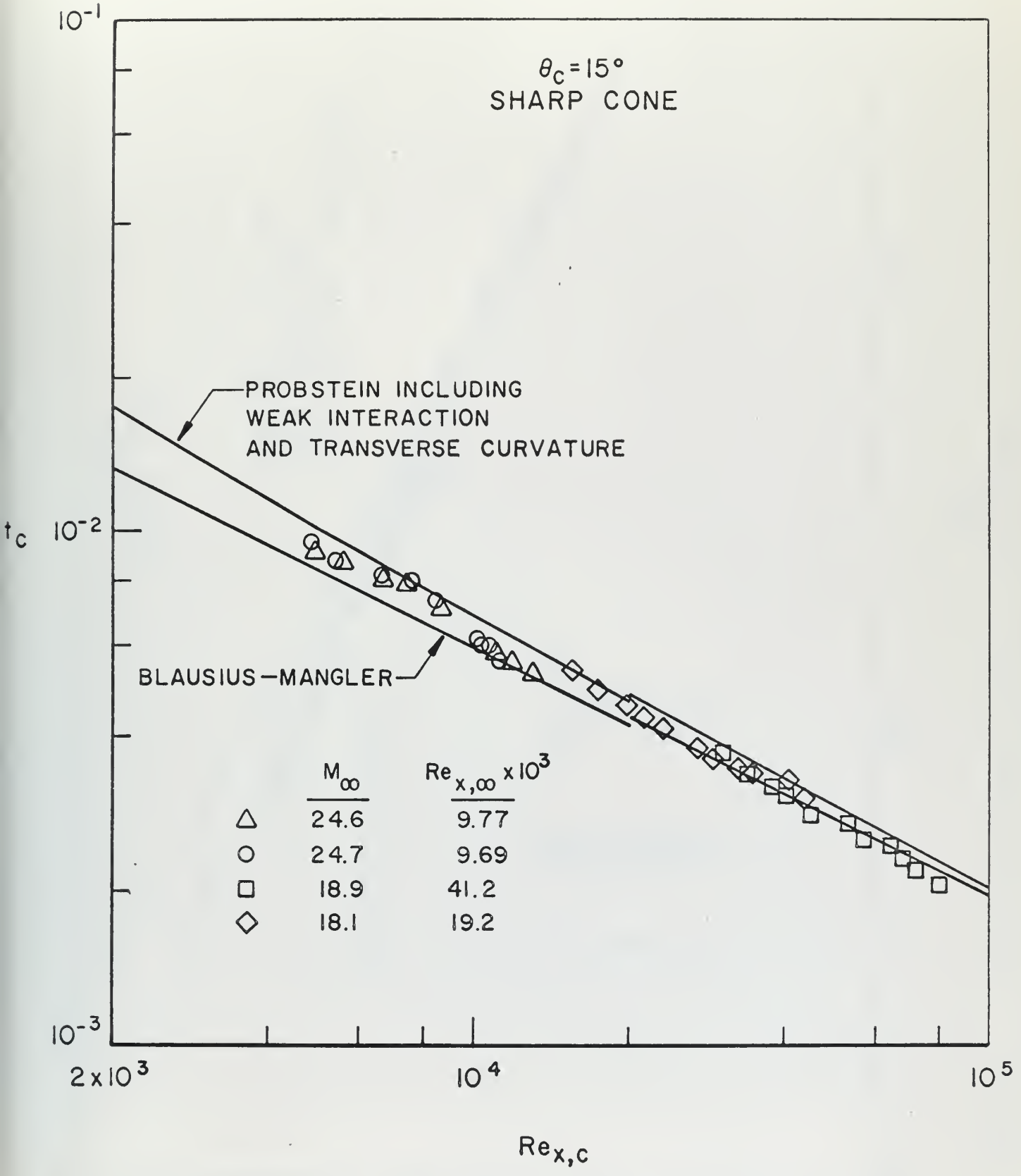

Figure 10 15° Sharp Cone Stanton Number vs. Reynolds Number

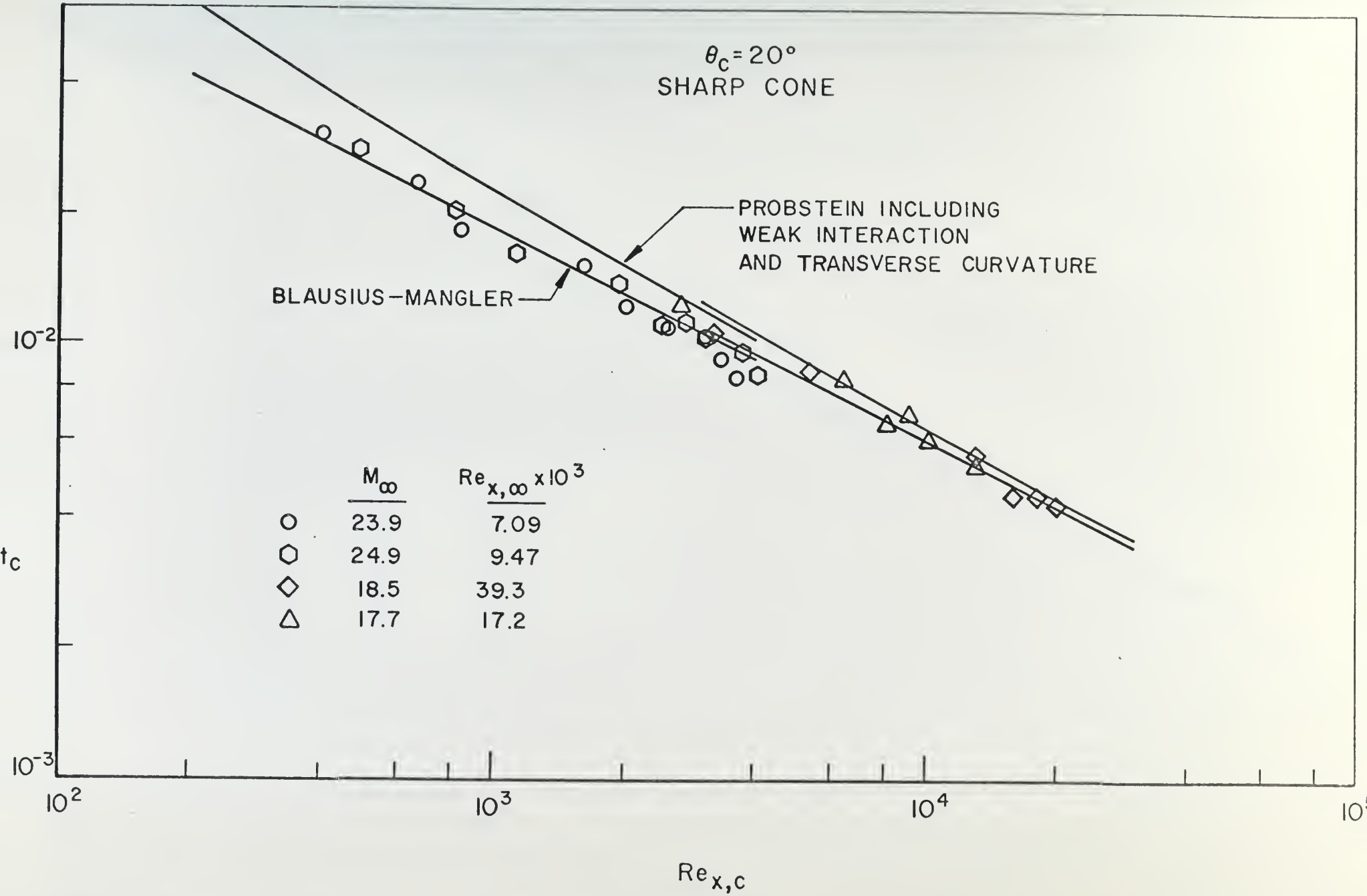

Figure 11 20° Sharp Cone Stanton Number vs. Reynolds Number

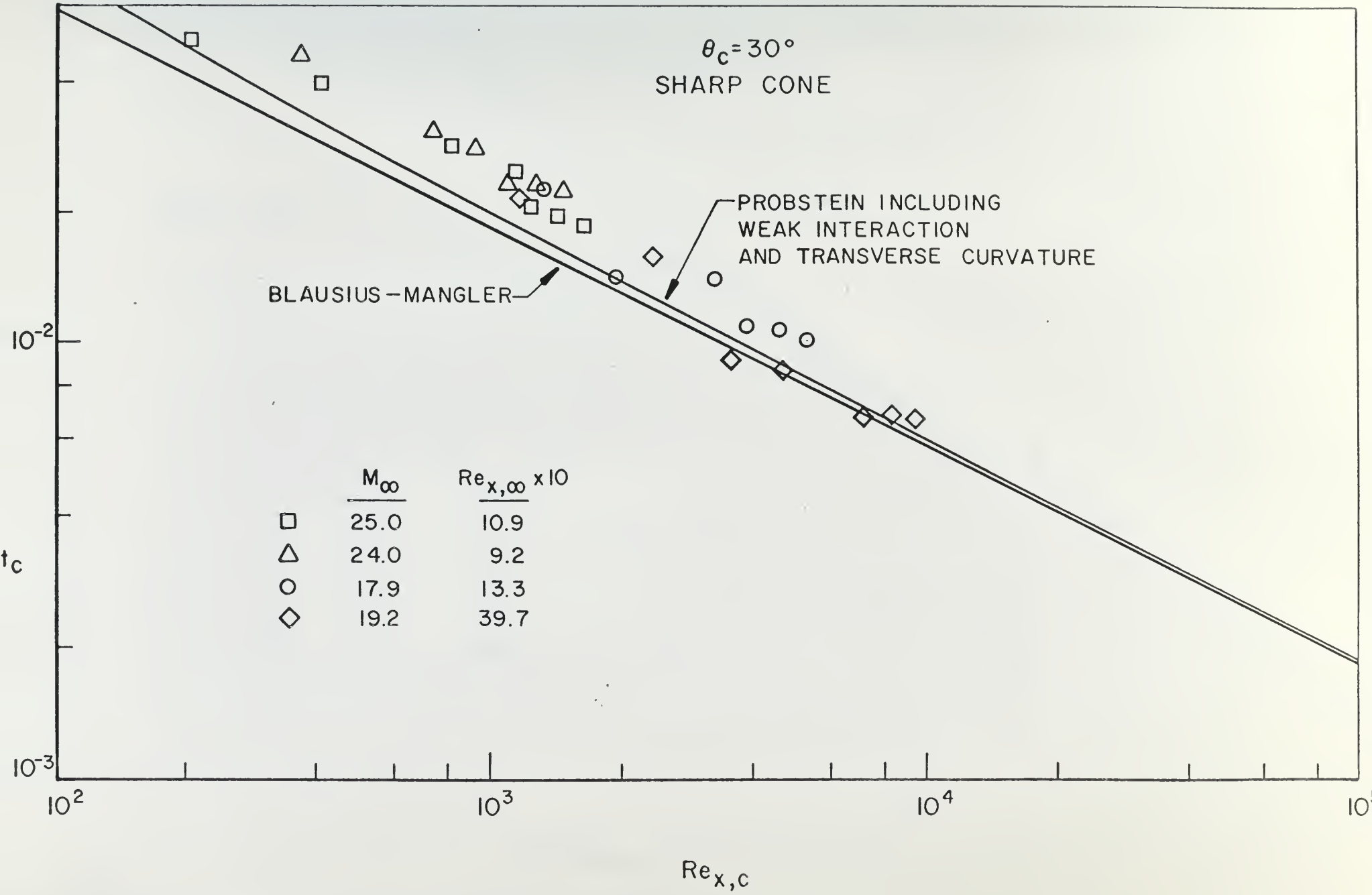

Figure 12 30° Sharp Cone Stanton Number vs. Reynolds Number

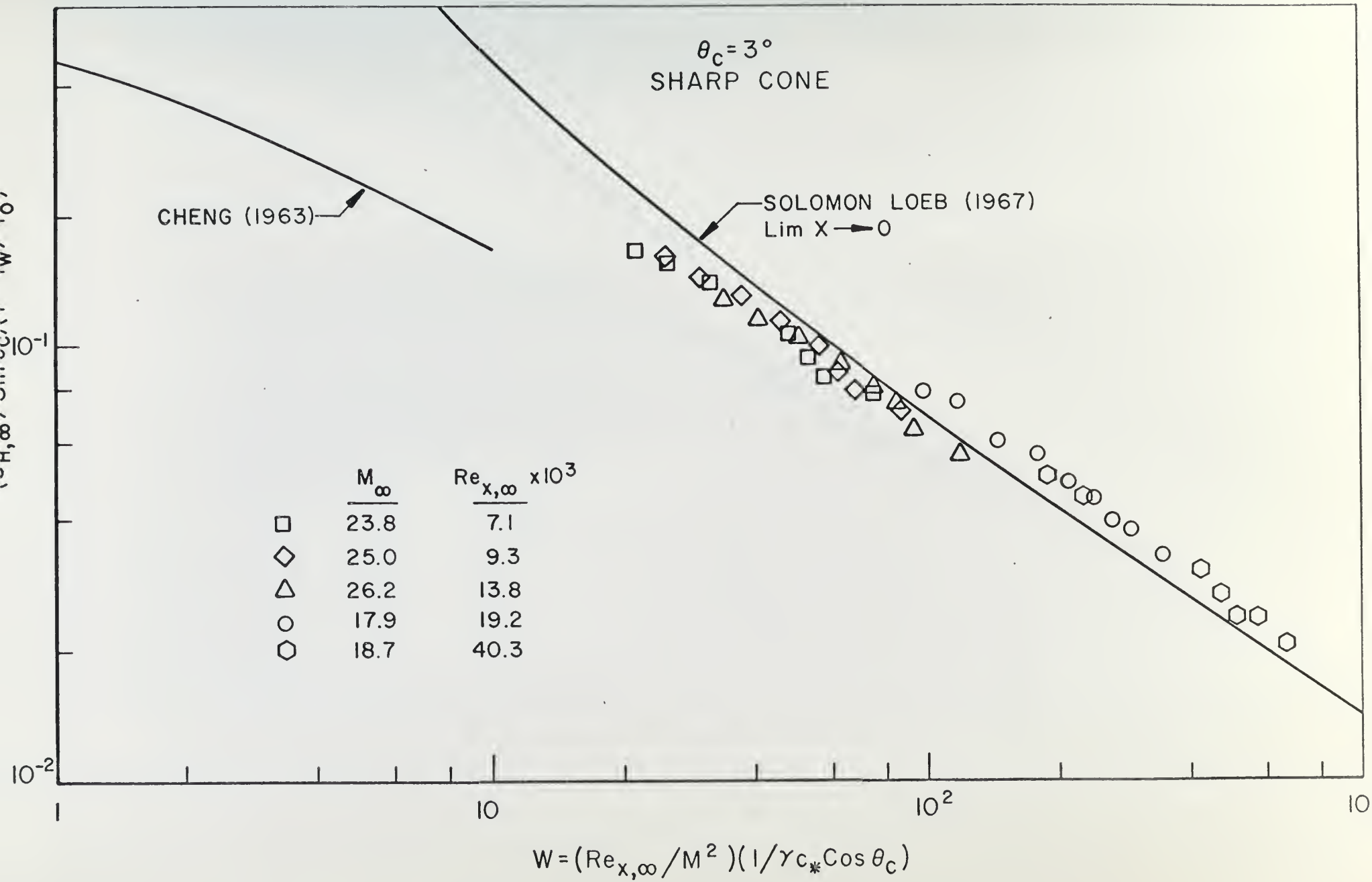

Figure 13 3° Sharp Cone Heat Transfer Parameters

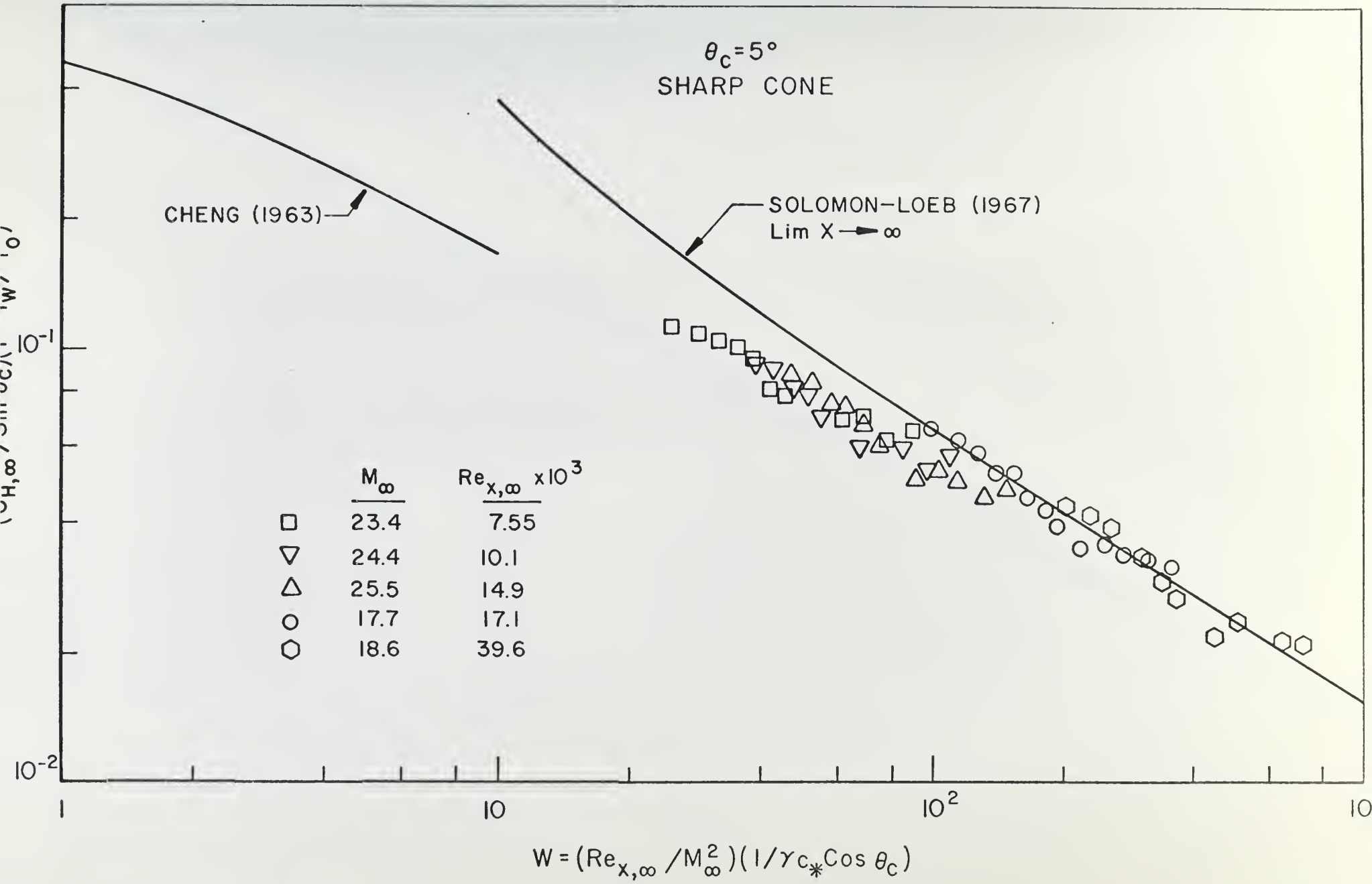

Figure 14 5° Sharp Cone Heat Transfer Parameters

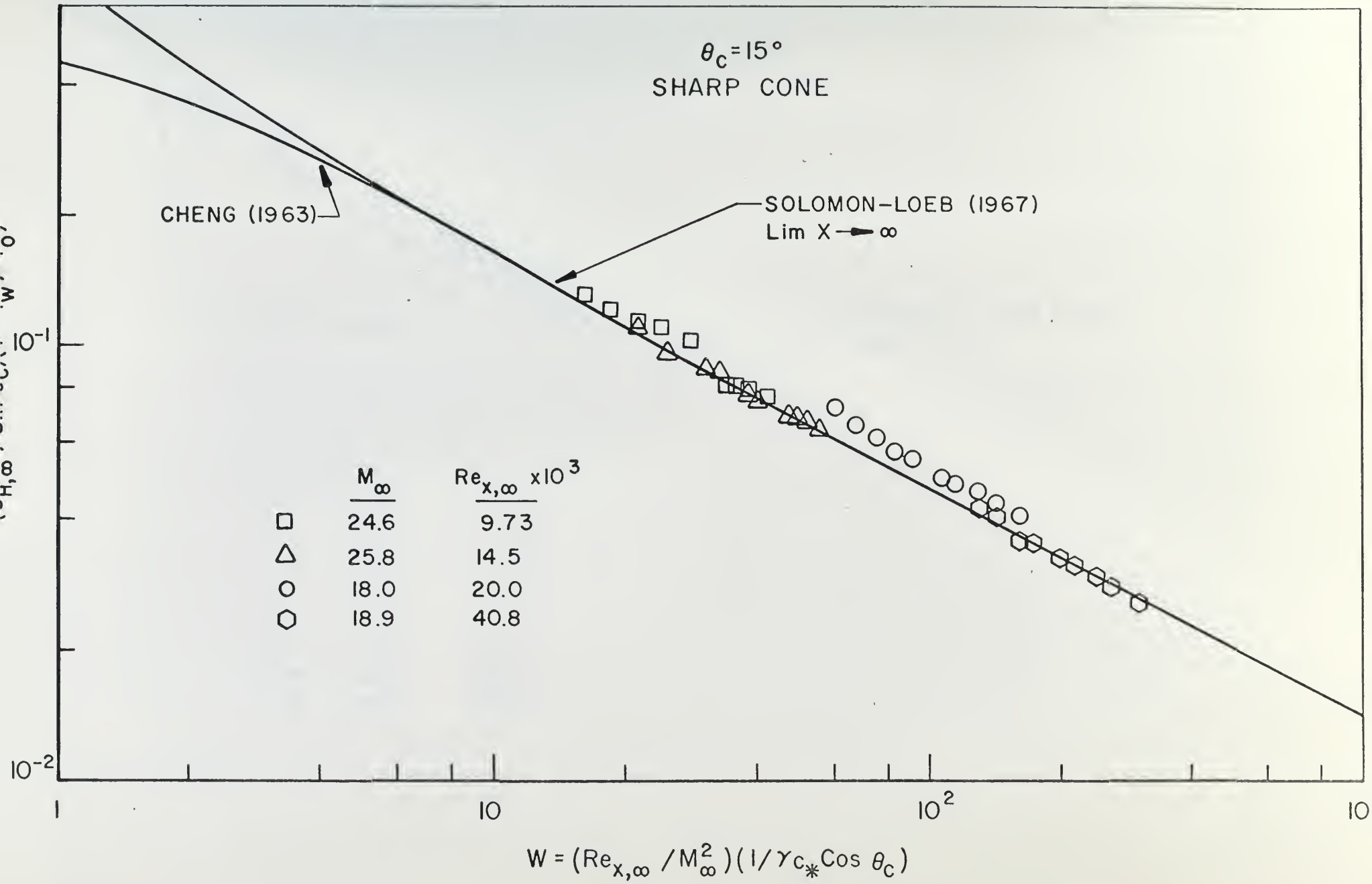

Figure 15 15° Sharp Cone Heat Transfer Parameters

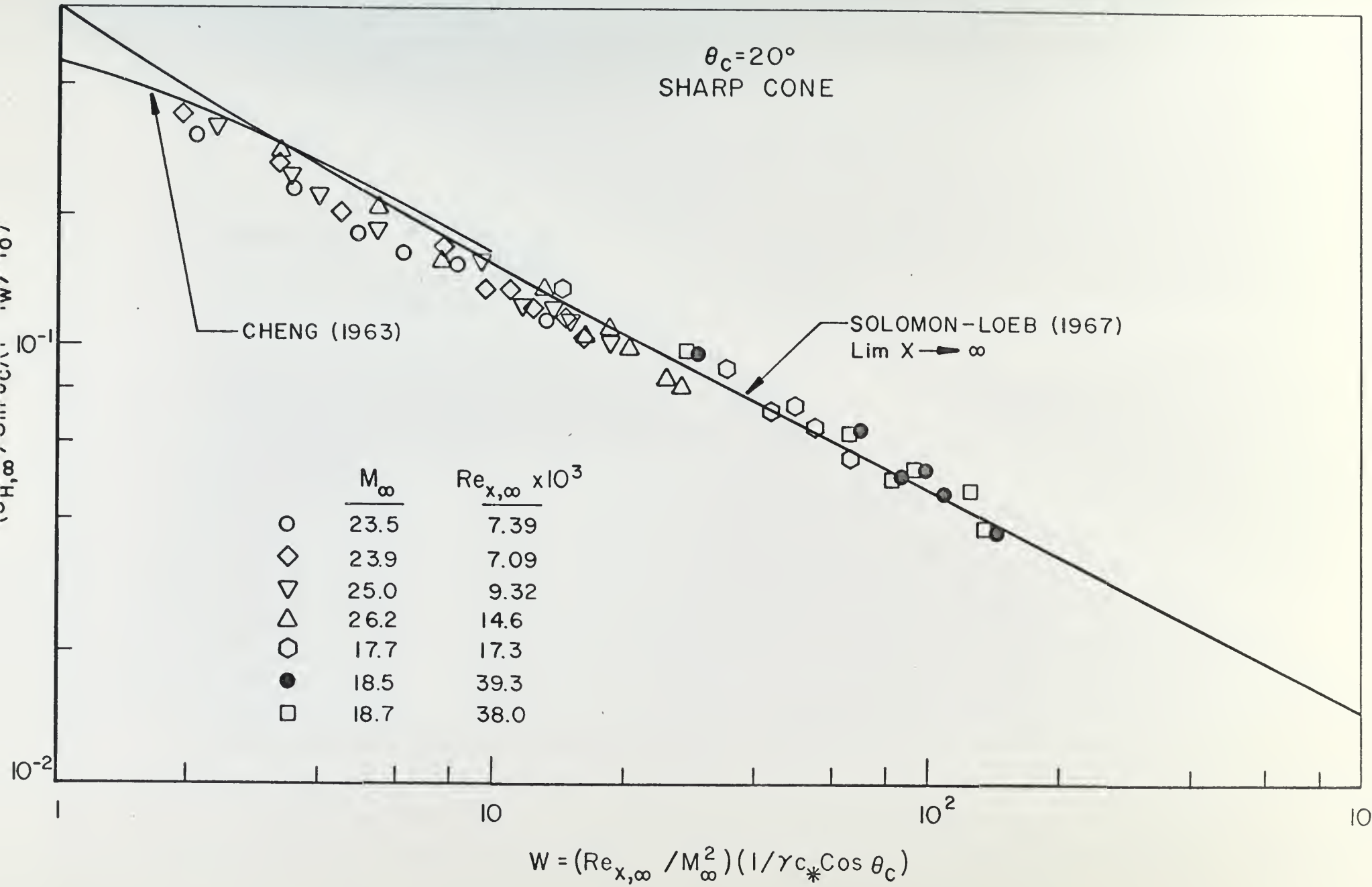

Figure 16 20° Sharp Cone [illegible]

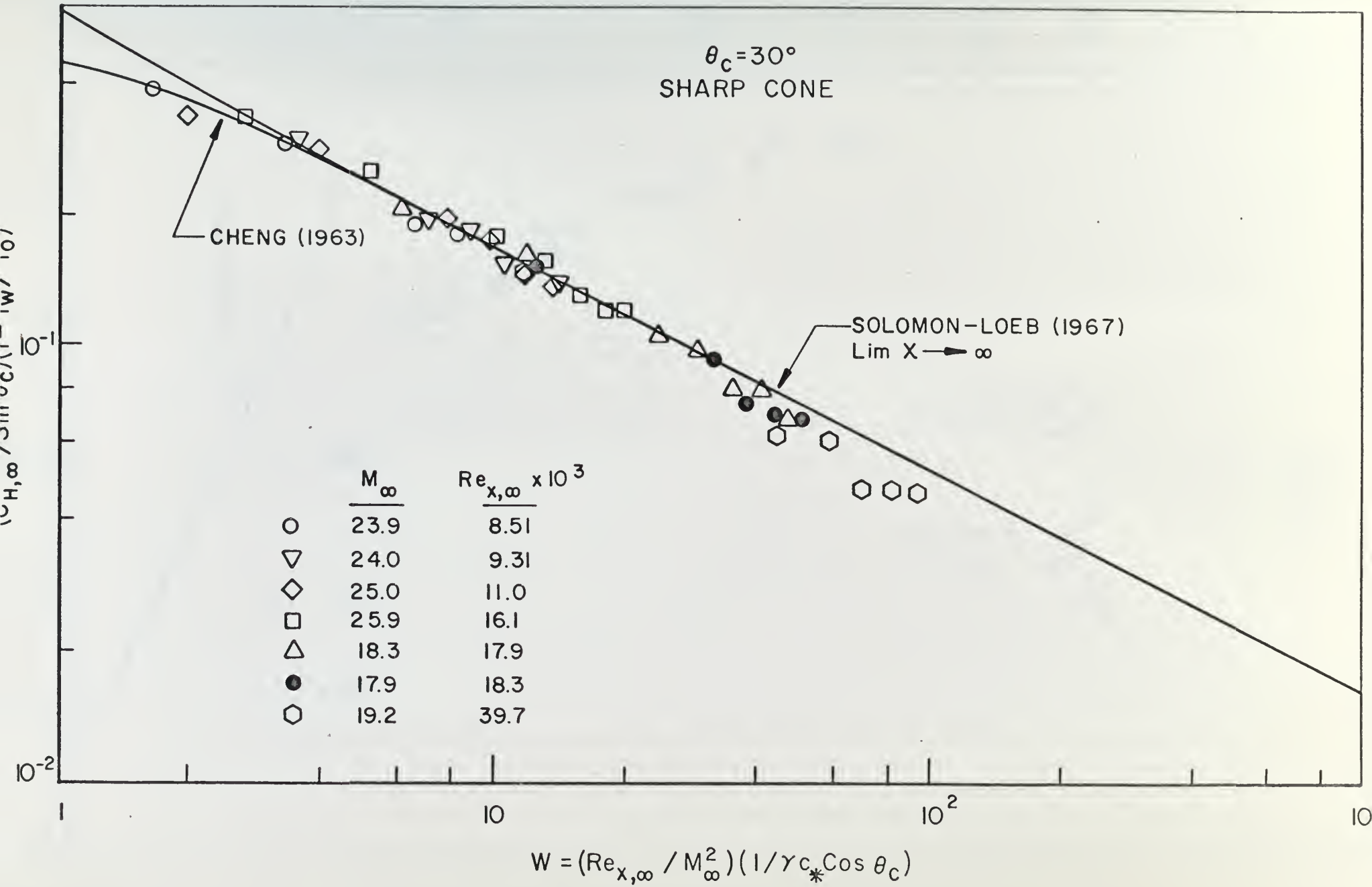

Figure 17 30° Sharp Cone Heat Transfer Parameters

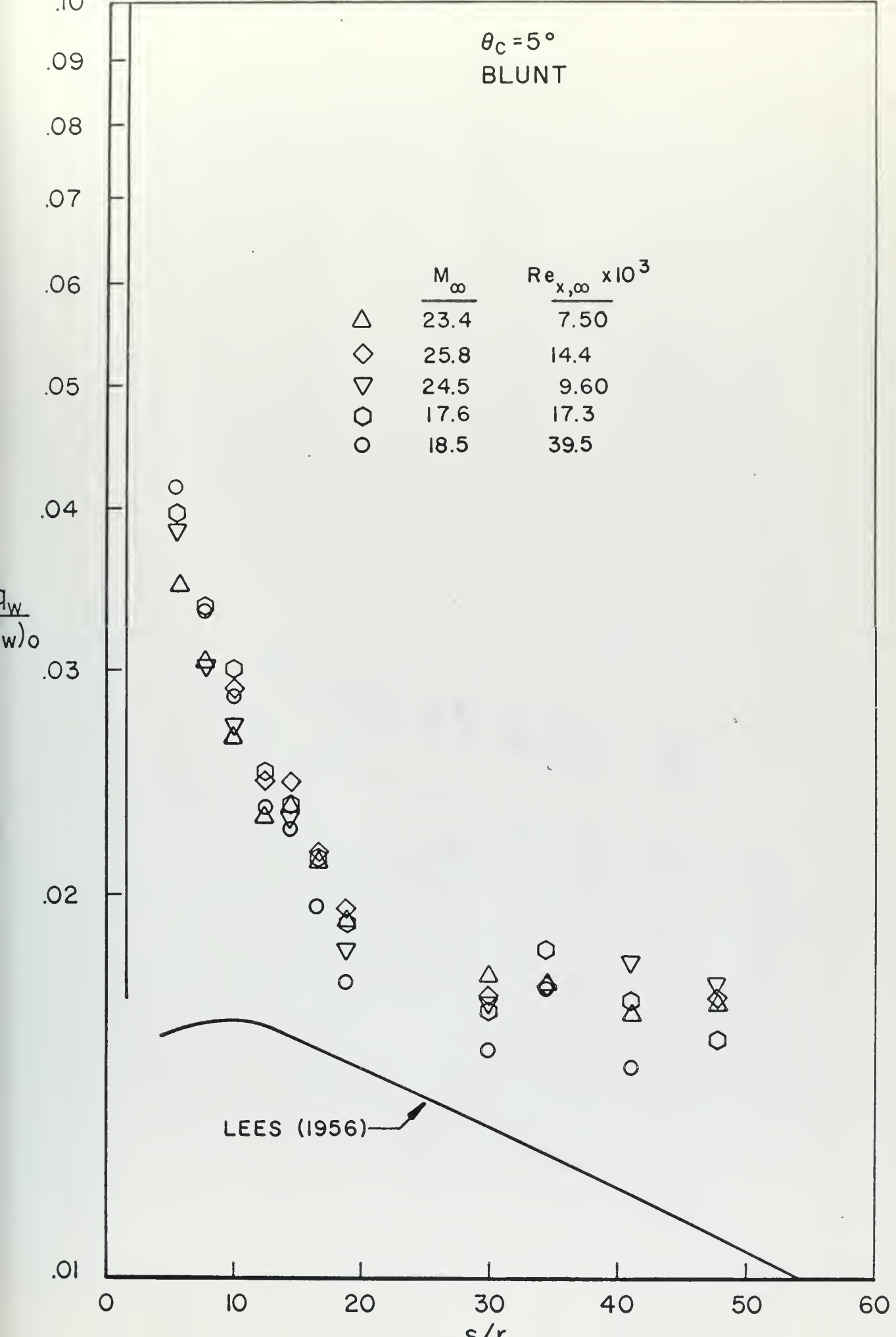

Figure 18 5° Blunt Cone Heat Flux Distribution

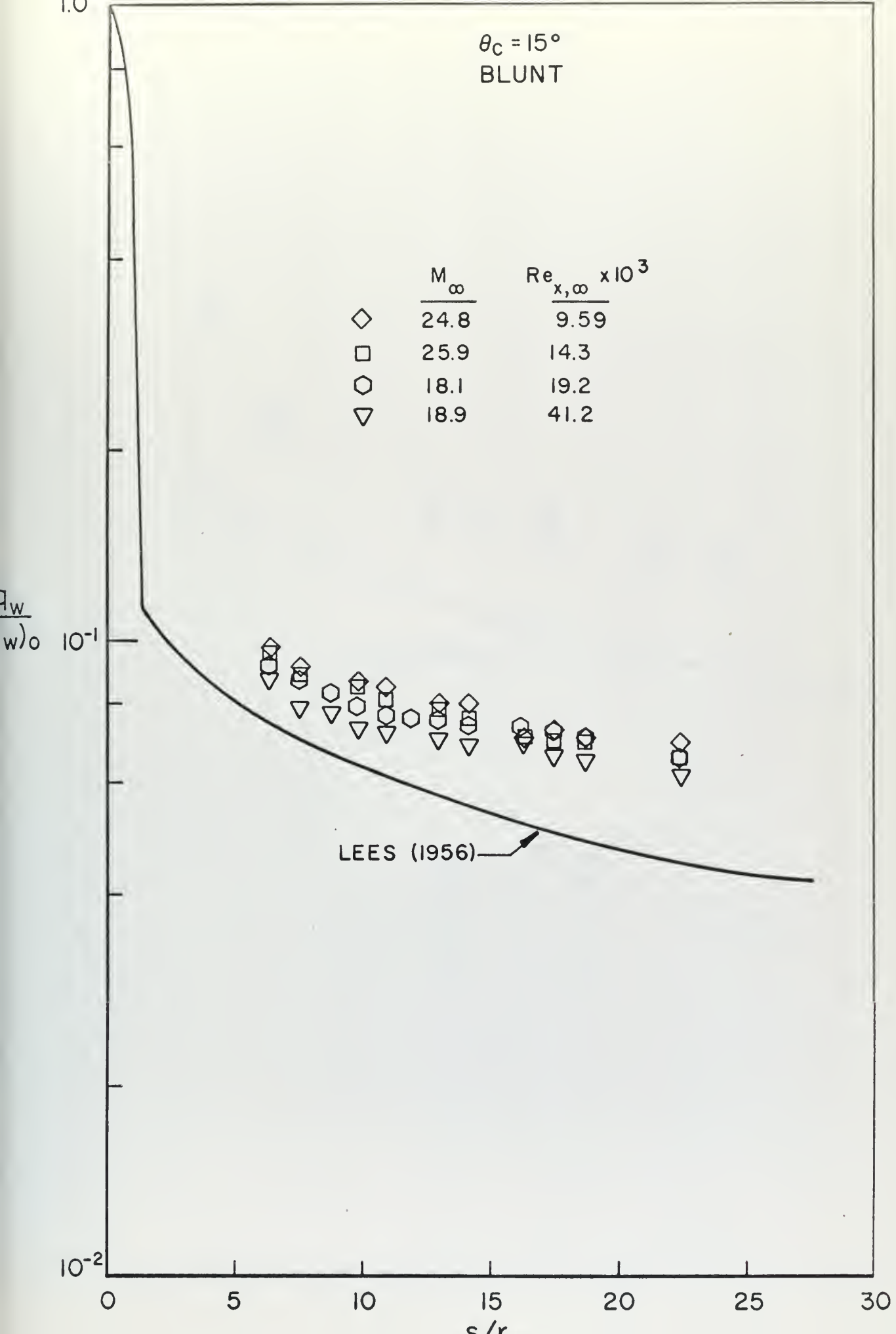

Figure 19 15° Blunt Cone Heat Flux Distribution

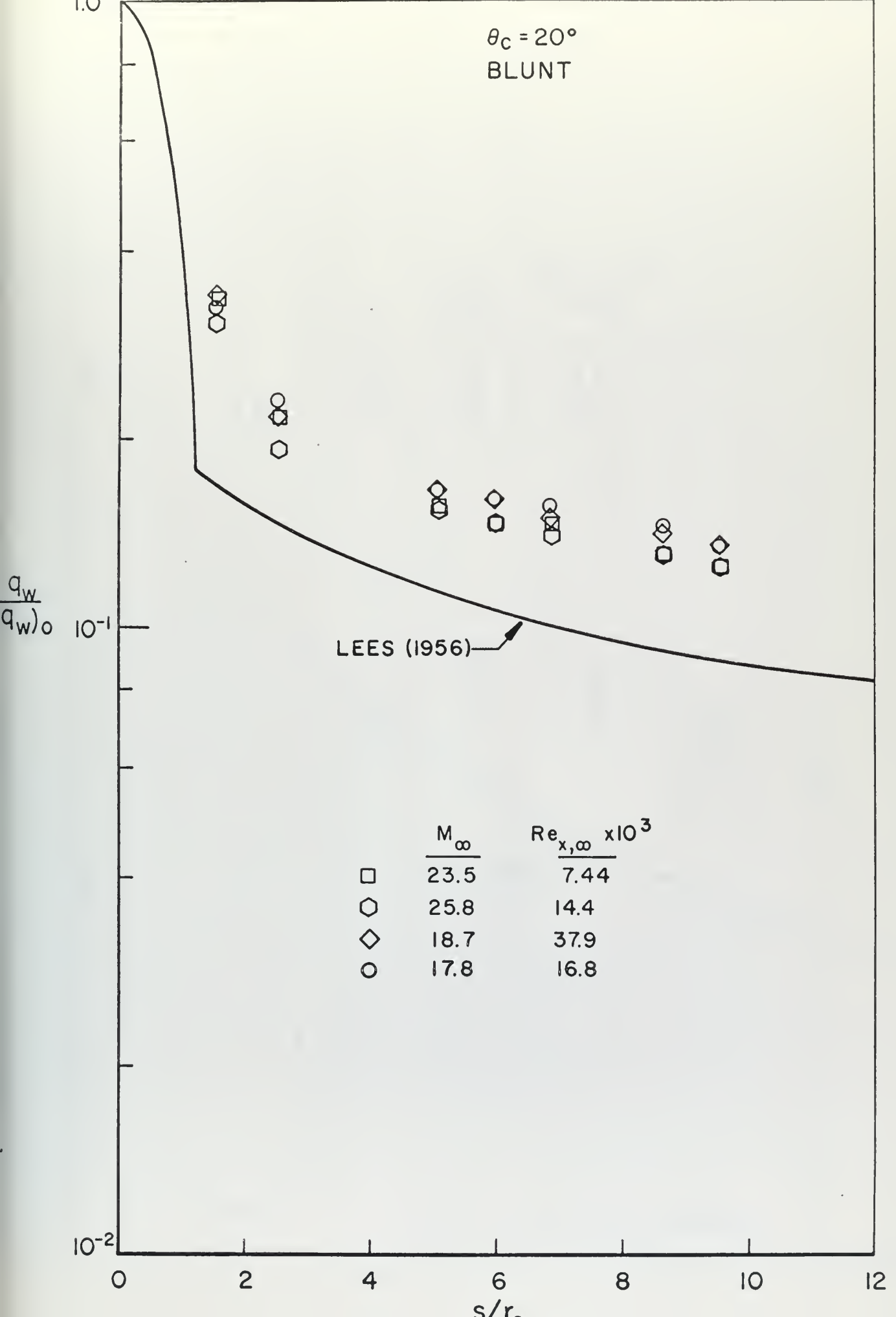

Figure 20 20° Blunt Cone Heat Flux Distribution

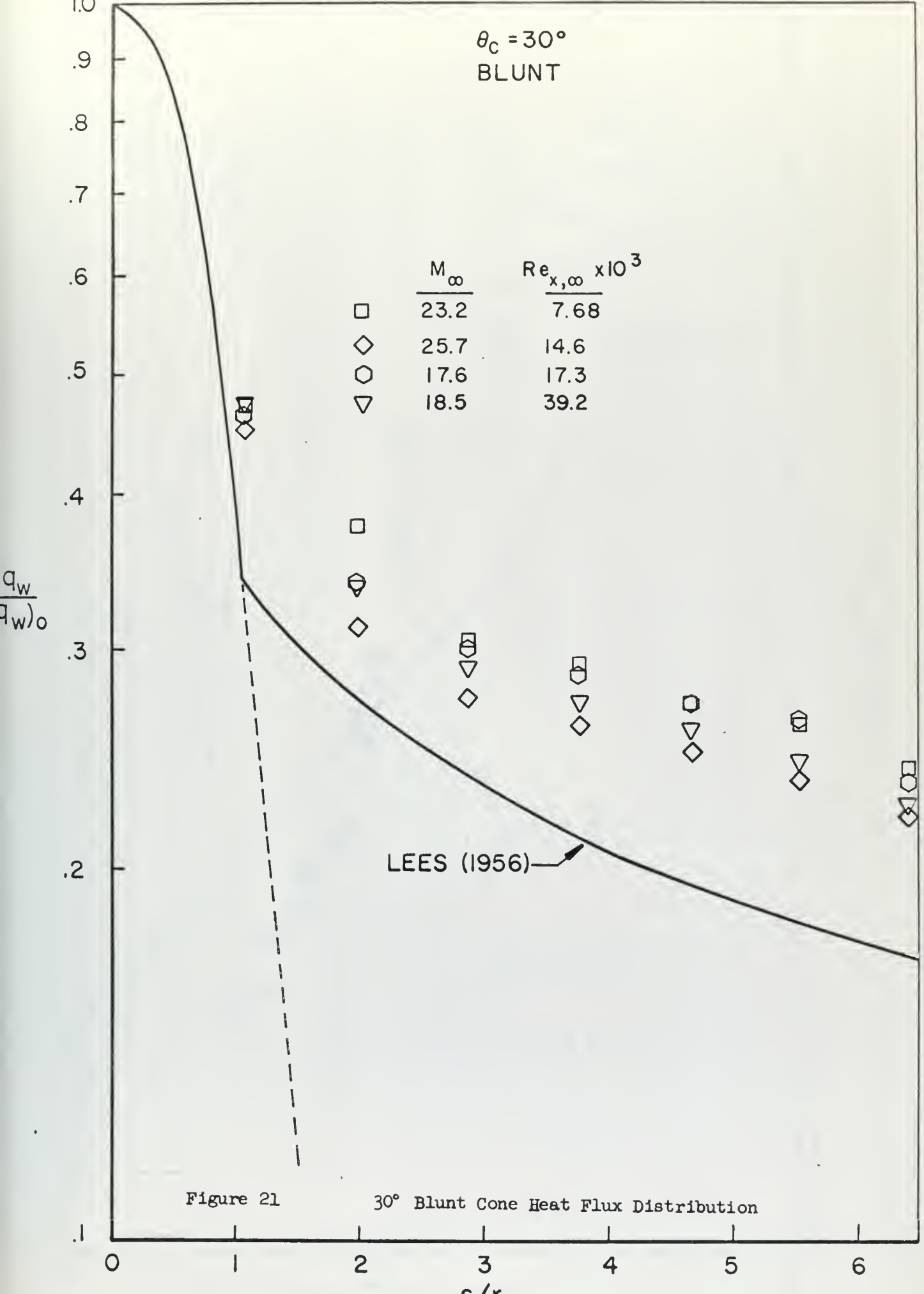

Figure 21 30° Blunt Cone Heat Flux Distribution

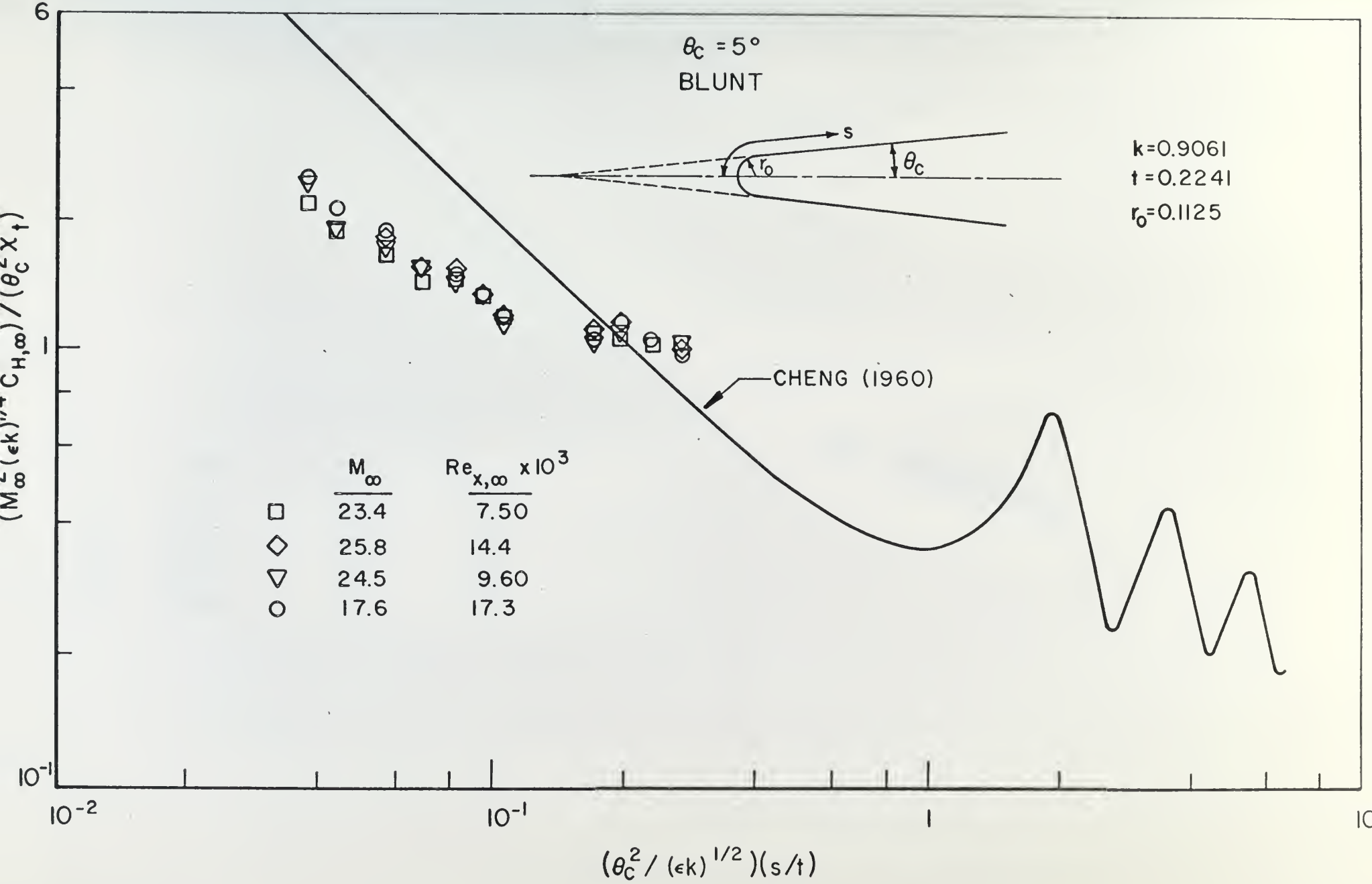

Figure 22 5° Blunt Cone Heat Transfer Parameters

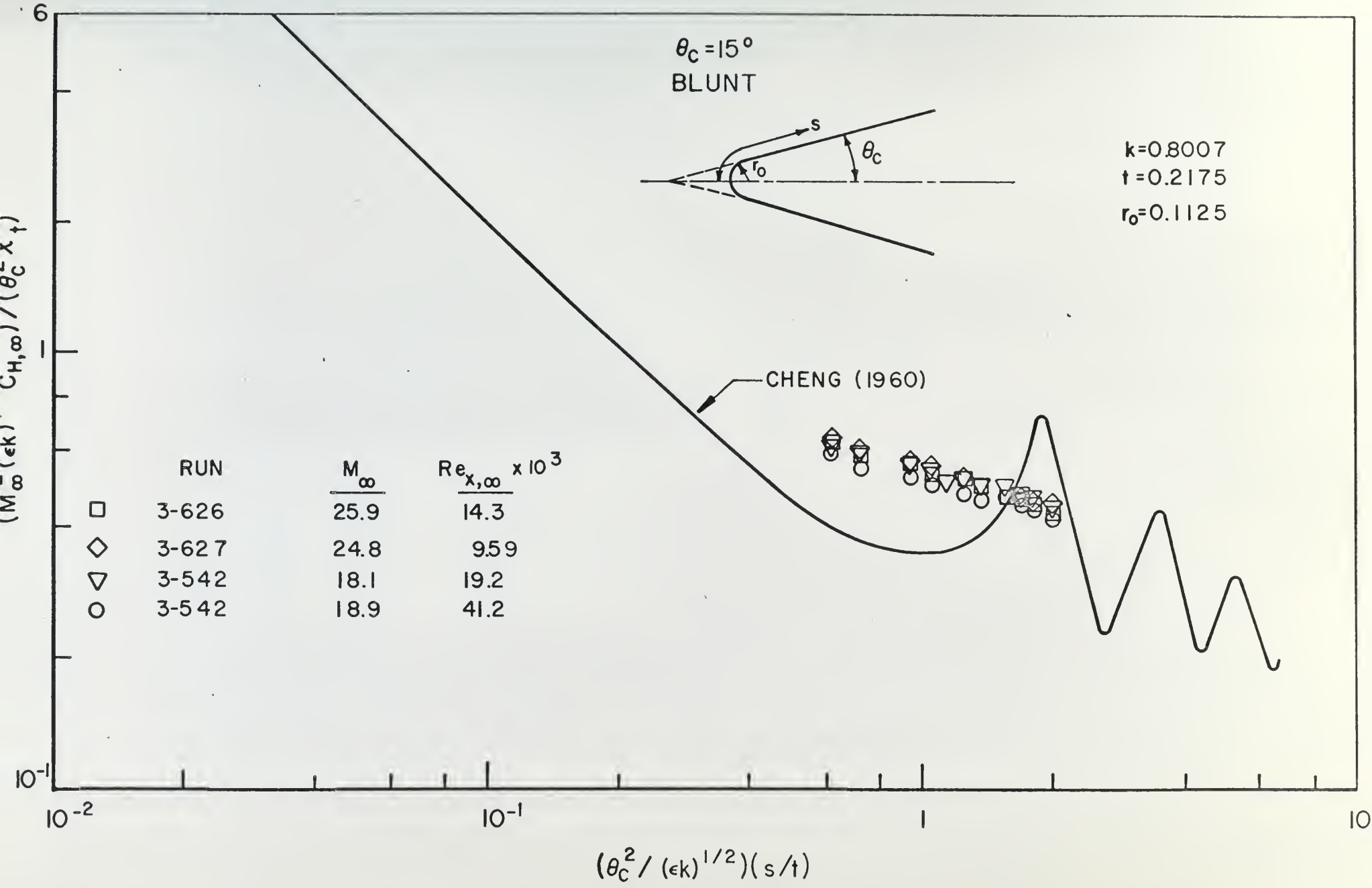

Figure 23 15° Blunt Cone Heat Transfer Parameters

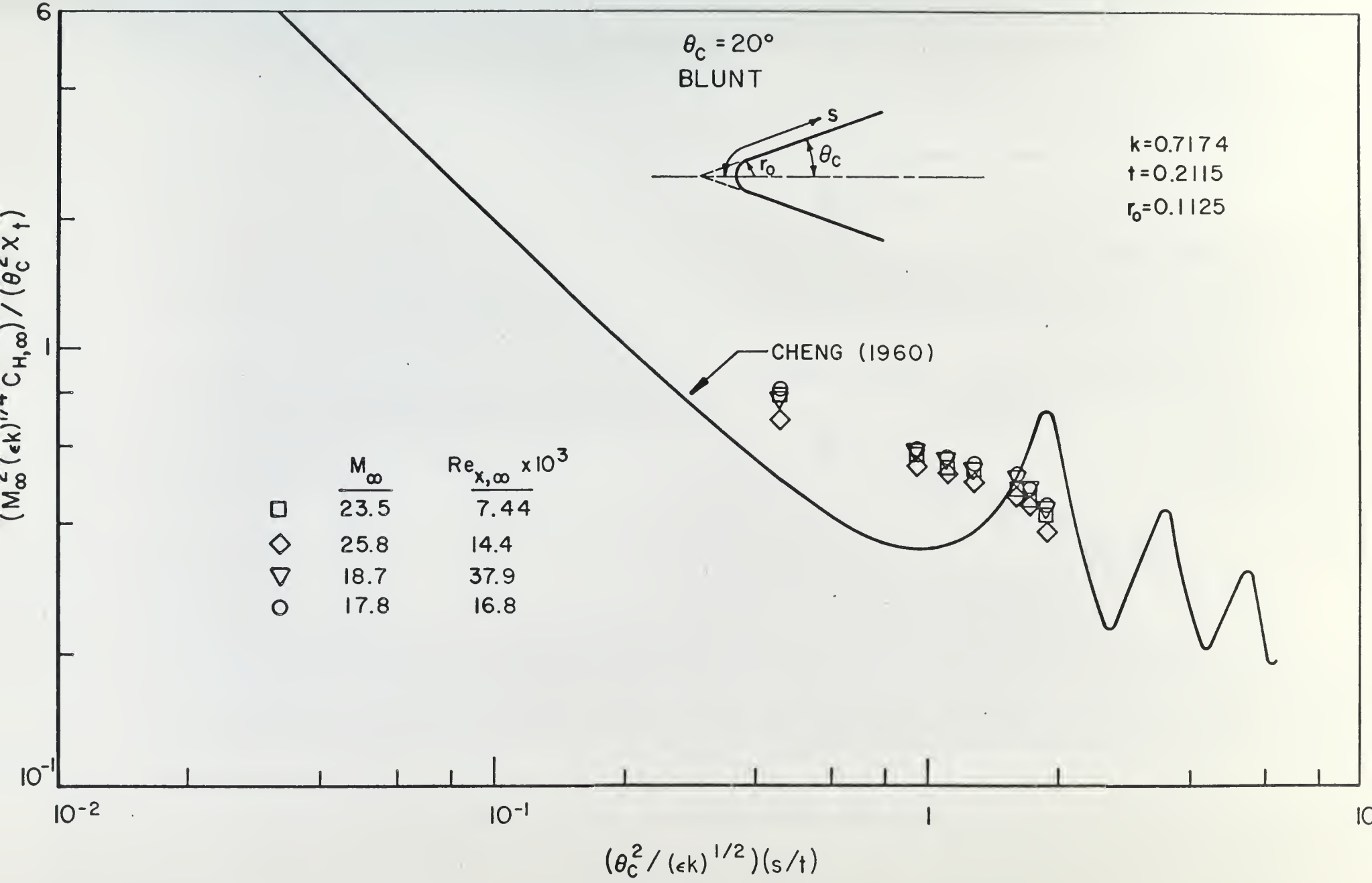

Figure 24 20° Blunt Cone Heat Transfer Parameters

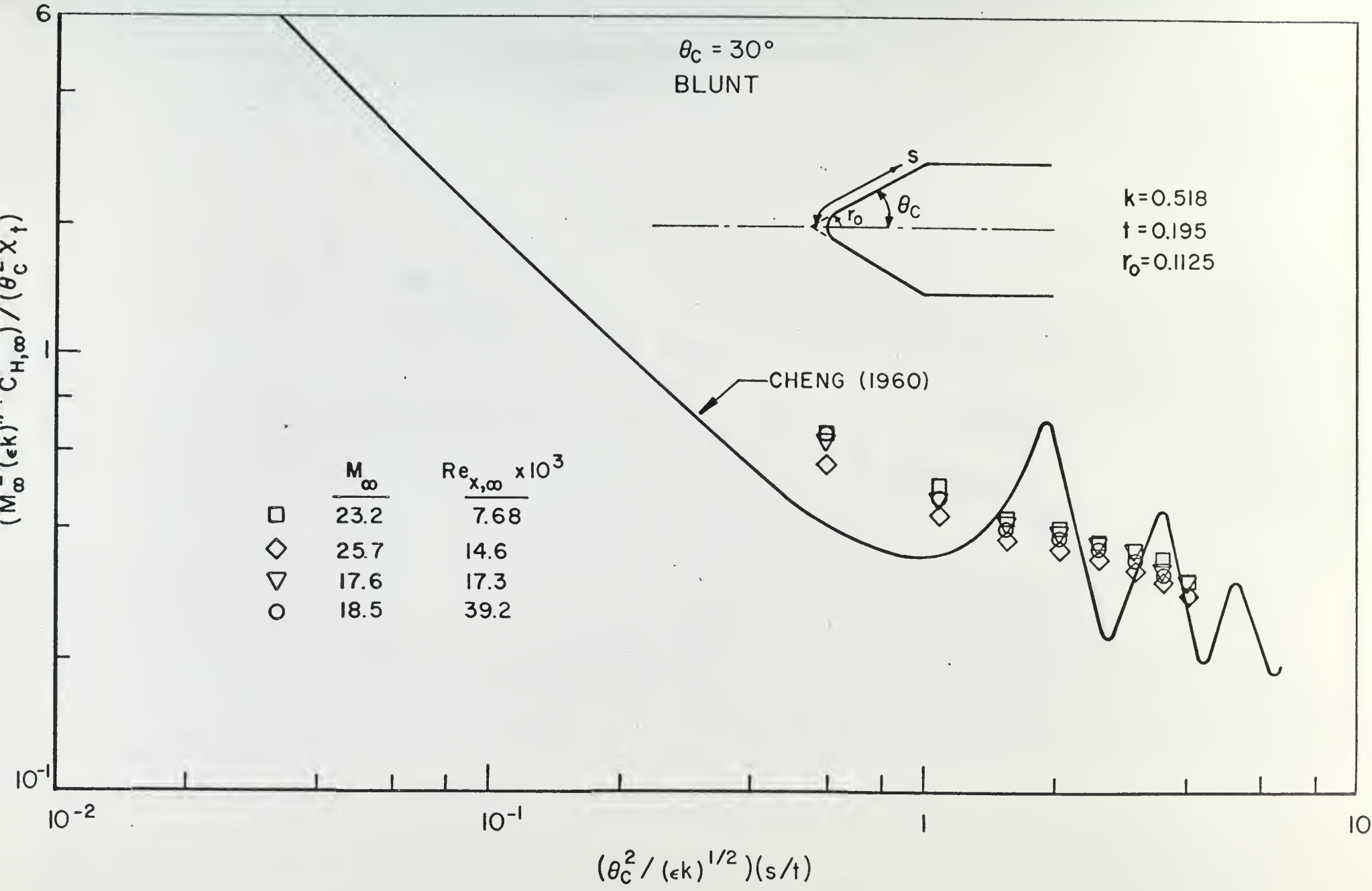

Figure 25 30° Blunt Cone Heat Transfer Parameters

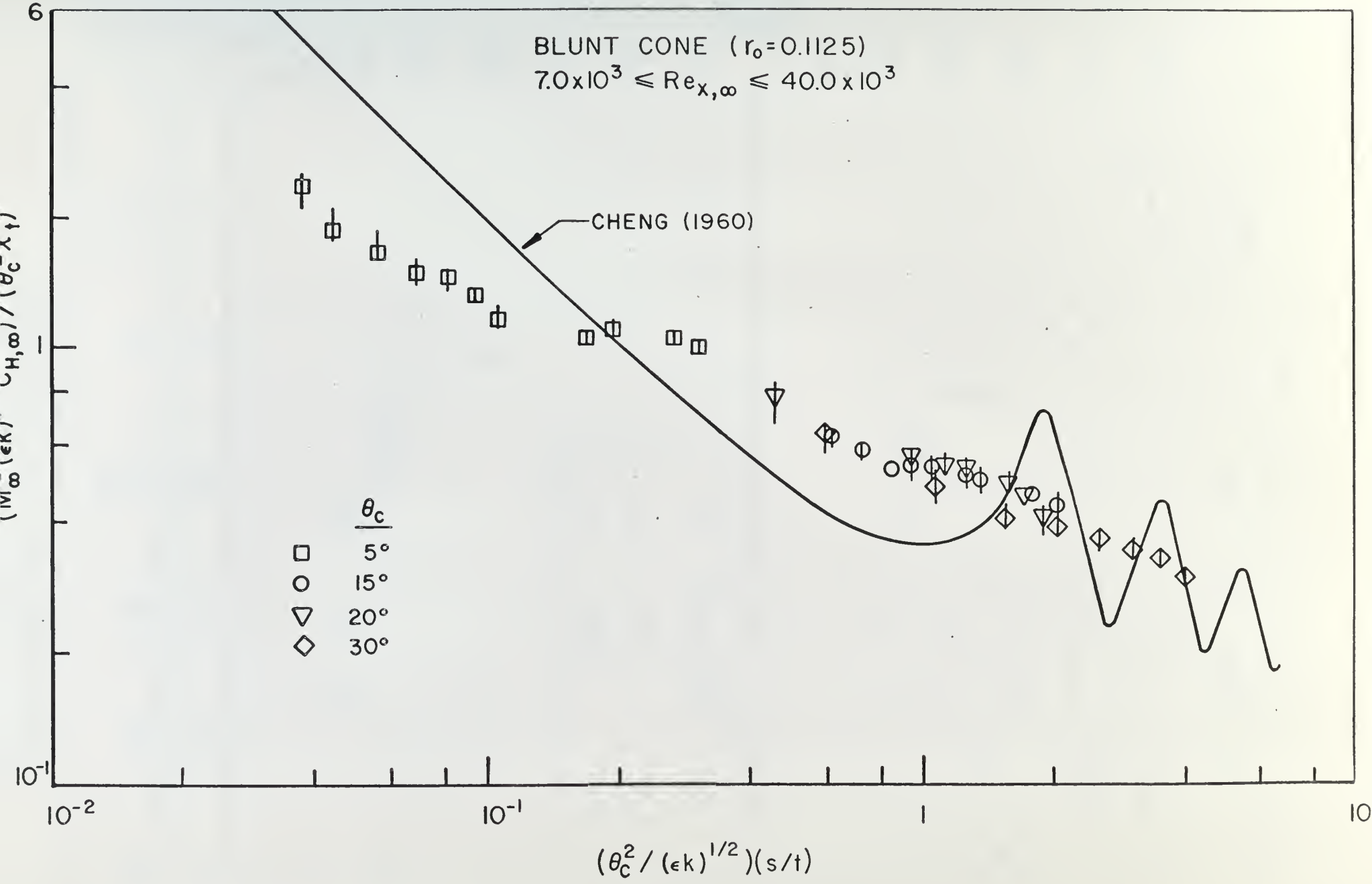

Figure 26 Combined Presentation of Blunt Cone Data

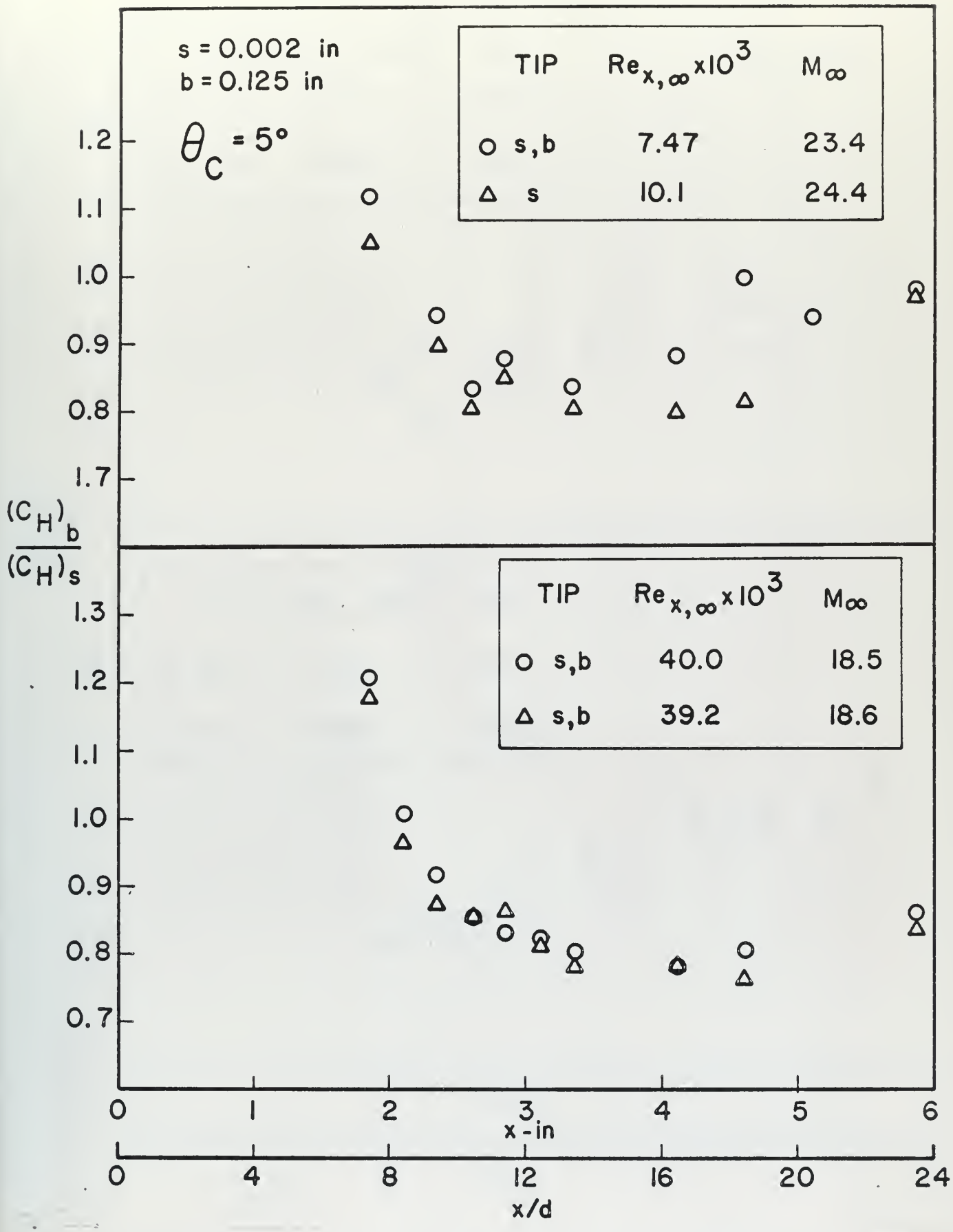

Figure 27 Ratio of Blunt Cone to Sharp Cone Heat Transfer Parameters for the 5° Cone at Equal Distances from the Virtual Tip

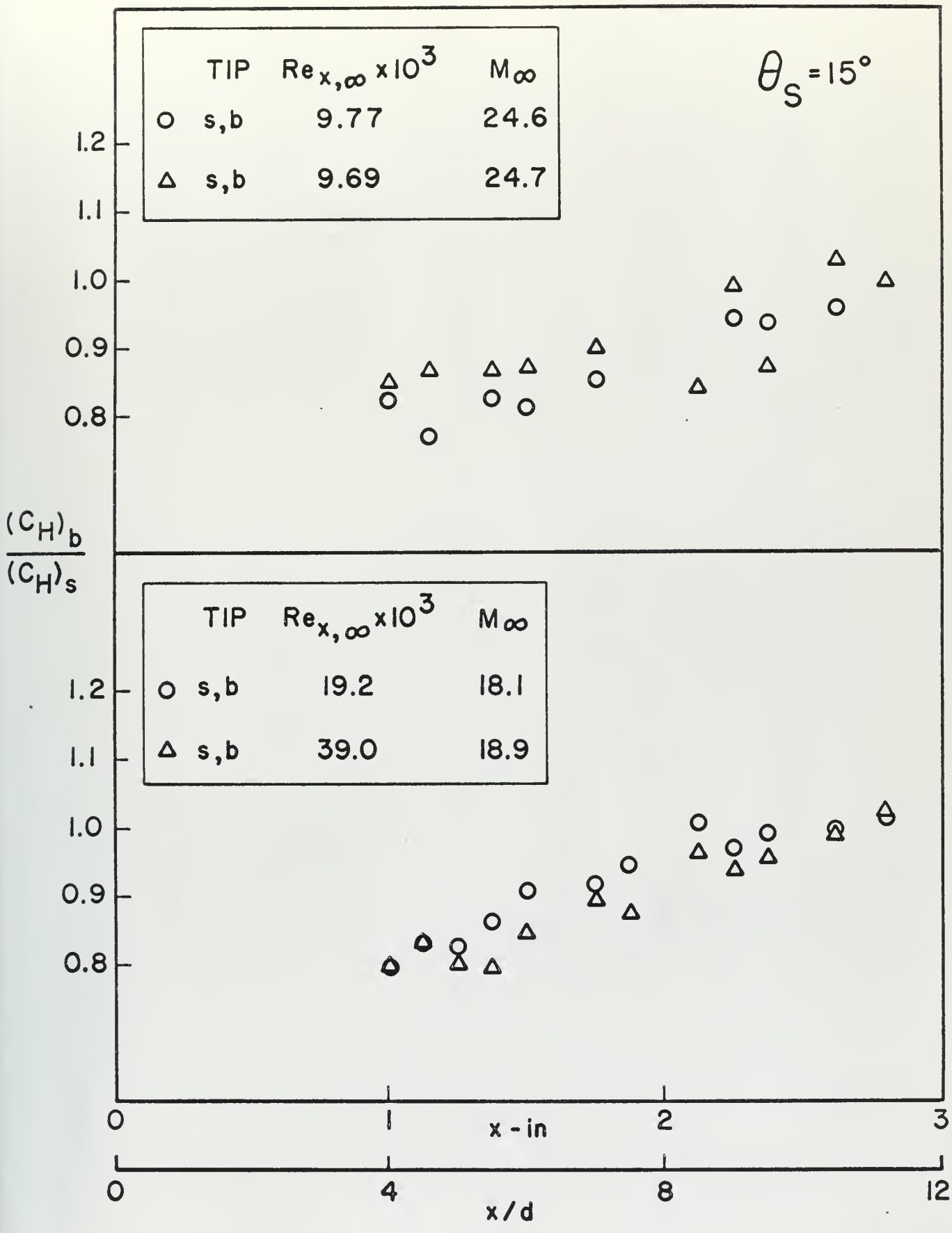

Figure 28 Ratio of Blunt Cone to Sharp Cone Heat Transfer Parameters for the 15° Cone at Equal Distances from the Virtual Tip

Thesis
B454 Berry
An experimental investigation of heat transfer to cones in rarified hypersonic flow.
130886